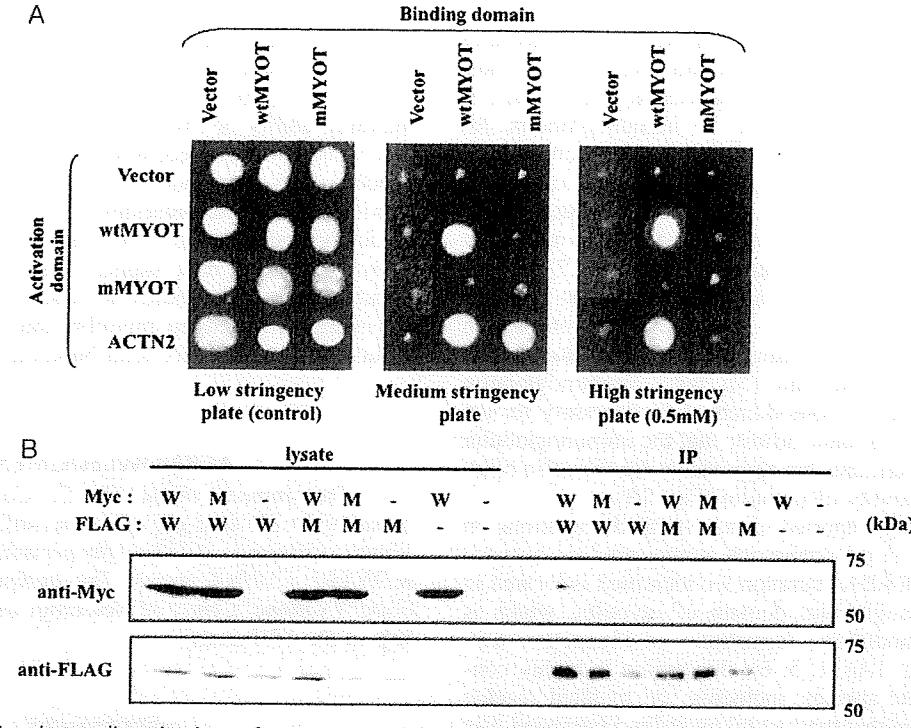

FIGURE 3. Defective homodimerization of mutant myotilin. **(A)** Yeast cells were cotransformed with expression plasmids containing Gal4 DNA-binding or activation domains alone (vector) or fused in frame to full-length human wild-type myotilin (wtMYOT), mutant myotilin (mMYOT), or α-actinin (ACTN2). Double transformants were first selected on low-stringency plates (used as control) and then spotted onto medium- and high-stringency plates. There is a lack of growth of cells coexpressing mMYOT and the corresponding constructs containing mMYOT and wtMYOT on medium- and high-stringency plates (0.5 mmol/L 3-amino-1,2,4-triazole [3-AT]). Cells cotransformed with mMYOT and ACTN2 did not grow on high-stringency plates (0.5 mmol/L 3-AT). **(B)** Myc-tagged myotilin and FLAG-tagged myotilin were coexpressed in COS-7 cells. The cell lysates were subjected to immunoprecipitation with an anti-FLAG M2 affinity gel. The immunoprecipitates (IP) were detected with anti-Myc (upper) or anti-FLAG (lower) antibodies. The mMYOT shows reduced interaction with both wild-type (W) and mutant (M) myotilin. −, empty vector transfected as a control.

and FLNC transformants grew on medium- and high-stringency plates (0.2–2 mmol/L 3-AT). By contrast, mMYOT and ACTN2 transformants grew on medium-stringency and high-stringency plates with 0.2 mmol/L 3-AT but did not grow on high-stringency plates with 0.5, 1, or 2 mmol/L 3-AT (Fig. 3A). This result indicates a decreased binding ability of mutant myotilin to α-actinin. In addition, mMYOT and FLNC transformants did not grow on medium- or high-stringency medium, but FLNC and mMYOT transformants grew on high-stringency medium when Gal4 DNA-binding domain construct containing FLNC was used as the bait (data not shown).

Immunoprecipitation Analysis of Homodimerization

We next used coimmunoprecipitation analysis to confirm the homodimerization defect of mutant myotilin. Myc-tagged wild-type myotilin (Myc-wtMYOT) coimmunoprecipitated with FLAG-tagged wild-type myotilin (FLAG-wtMYOT); this indicates that wild-type myotilin forms a homodimer. On the other hand, other combinations of FLAG-wtMYOT and Myc-tagged mutant myotilin (Myc-mMYOT), FLAG- mMYOT and Myc-wtMYOT, and FLAG-mMYOT and Myc-mMYOT showed decreased interaction (Fig. 3B). These results suggest that the p.R405K mutation in the second immunoglobulin-like domain of myotilin can affect the homodimerization ability of myotilin protein.

DISCUSSION

Limb girdle muscular dystrophy type 1A is an autosomal-dominant muscular dystrophy characterized by progressive proximal muscle weakness and wasting. Distal muscle weakness may occur later (12, 13). The *MYOT* mutations are known to cause LGMD1A, but only a few genetically confirmed LGMD1A patients have been reported to date. Here, we report the first *MYOT* mutation in the Japanese population. The patient had a clinical severity similar to that in other reported LGMD1A patients, and there was also disorganization of myofibrils and rimmed vacuoles in the muscle biopsy tissue. Immunohistochemical analysis revealed accumulation of Z disk proteins (i.e. myotilin, αB-crystallin, ZASP, desmin, and actin) as seen in MFM, thus highlighting the similarities in the pathology of LGMD1A and MFM (21).

Myotilin has 2 immunoglobulin domains in the C terminus of the molecule. Several cytoskeletal proteins have been shown to contain immunoglobulin domains, and most of these proteins are specifically expressed in striated muscle, suggesting a special function for the immunoglobulin domains in this tissue (13, 22). Immunoglobulin domains are known to mediate protein-protein interactions and to serve as dimerization sites and regulators for molecular elasticity and act as modular "spacers" that place an interacting module in the correct position for performing its function (1, 7, 22, 23). The functional importance of the immunoglobulin domains in myotilin was demonstrated by introducing myotilin with mutant immunoglobulin domains in yeast cells that do not express endogenous myotilin (5); these immunoglobulin domains are the site for homodimerization necessary for the actin bundling (8). Our data indicate that the immunoglobulin domains in the C terminus are responsible for the actin binding and bundling ability of myotilin (Fig. 3B).

All previously reported disease-related mutations in *MYOT* are located in the serine-rich amino-terminus of myotilin. The novel p.R405K mutation we identified is located in the second immunoglobulin domain of myotilin, which is important for homodimeric formation and interaction with other proteins (Fig. 1A) (1, 5, 6); this region is highly conserved in vertebrate species, including the mutated residue (Fig. 1B). We found that the 110-kd myotilin dimer band was faint in the patient's muscle sample by immunoblotting, although, as in a previous report (24), the amount of myotilin in the patient's muscle sample was increased. Furthermore, the decreased homodimerization ability of mutant (p.R405K) myotilin was confirmed by the Y2H and immunoprecipitation studies in which interactions of mutant myotilin with both wild-type and mutant myotilin were greatly reduced (Figs. 3A, B). These results suggest that the disturbance of homodimerization caused by the mutated allele may affect the actin-bundling ability of myotilin at the Z disks, resulting in decreased filament stability and gradual disruption in the Z disk in vivo.

Myotilin interacts with 2 important actin-bundling (cross-linker) proteins (i.e. α-actinin and FLNC), forming a complex of 3 actin bundlers at the Z disk. Previous experiments have shown that myotilin enhances the binding of α-actinin to actin (8). The decreased binding ability of mutated myotilin to α-actinin we observed suggests that this altered interaction may loosen the complex formed by these actin bundler proteins leading to a decrease in strength and ability of the Z disk to resist mechanical stress during muscle contraction. On the other hand, mutant myotilin showed no apparent defect in interaction with actin but questionable defective interaction with FLNC by Y2H assay; this issue requires further analysis.

Several hypotheses have been proposed regarding the pathogenesis of the previously reported *MYOT* mutations in Exon 2, including the fact that the serine-rich domain contains a hydrophobic stretch that mediates the localization of small amounts of myotilin to the sarcolemmal membrane. *MYOT* mutations may elongate this hydrophobic stretch, possibly disturbing its interactions with the sarcolemmal membrane (12). It has also been suggested that these mutations may disrupt the binding of myotilin with α-actinin, FLNC, or a novel protein-binding partner (12). None of these hypotheses have been proven. Disease-associated substitutions in myotilin did not affect the localization or actin-bundling ability of myotilin, suggesting that the pathogenic mechanism of the myotilin mutations examined may be independent of its actin-modulating effects (5). In contrast to the previously reported mutations (5, 13), ours is the first report to demonstrate a functional abnormality caused by mutated myotilin. Our data suggest that the p.R405K missense mutation disrupts myotilin homodimerization and decreases the interaction between myotilin and α-actinin, which subsequently may affect its actin-bundling ability.

ACKNOWLEDGMENTS

The authors thank Dr O. Carpén (University of Helsinki) for the kind gift of anti-myotilin antibody and Dr S. Ishiura (University of Tokyo) for providing the FLAG-inserted pcDNA3.1 V5/HisA vector. The authors also thank Dr R. Gabor (National Center of Neurology and Psychiatry) for his help in the Y2H assay.

REFERENCES

1. Salmikangas P, Mykkanen OM, Gronholm M, et al. Myotilin, a novel sarcomeric protein with two Ig-like domains, is encoded by a candidate gene for limb-girdle muscular dystrophy. Hum Mol Genet 1999;8:1329–36
2. Parast MM, Otey CA. Characterization of palladin, a novel protein localized to stress fibers and cell adhesions. J Cell Biol 2000;150:643–56
3. Mykkanen OM, Gronholm M, Ronty M, et al. Characterization of human palladin, a microfilament-associated protein. Mol Biol Cell 2001;12:3060–73
4. Bang ML, Mudry RE, McElhinny AS, et al. Myopalladin, a novel 145-kilodalton sarcomeric protein with multiple roles in Z-disc and I-band protein assemblies. J Cell Biol 2001;153:413–27
5. von Nandelstadh P, Gronholm M, Moza M, et al. Actin-organising properties of the muscular dystrophy protein myotilin. Exp Cell Res 2005;310:131–39
6. van der Ven PF, Wiesner S, Salmikangas P, et al. Indications for a novel muscular dystrophy pathway. Gamma-filamin, the muscle-specific filamin isoform, interacts with myotilin. J Cell Biol 2000;151:235–48
7. Gontier Y, Taivainen A, Fontao L, et al. The Z-disc proteins myotilin and FATZ-1 interact with each other and are connected to the sarcolemma via muscle-specific filamins. J Cell Sci 2005;118:3739–49
8. Salmikangas P, van der Ven PF, Lalowski M, et al. Myotilin, the limb-girdle muscular dystrophy 1A (LGMD1A) protein, cross-links actin filaments and controls sarcomere assembly. Hum Mol Genet 2003;12:189–203
9. Selcen D, Engel AG. Mutations in myotilin cause myofibrillar myopathy. Neurology 2004;62:1363–71
10. Foroud T, Pankratz N, Batchman AP, et al. A mutation in myotilin causes spheroid body myopathy. Neurology 2005;65:1936–40
11. Olivé M, Goldfarb LG, Shatunov A, et al. Myotilinopathy: Refining the clinical and myopathological phenotype. Brain 2005;128:2315–26
12. Hauser MA, Conde CB, Kowaljow V, et al. Myotilin mutation found in second pedigree with LGMD1A. Am J Hum Genet 2002;71:1428–32
13. Hauser MA, Horrigan SK, Salmikangas P, et al. Myotilin is mutated in limb girdle muscular dystrophy 1A. Hum Mol Genet 2000;9:2141–47
14. Penisson-Besnier I, Talvinen K, Dumez C, et al. Myotilinopathy in a family with late onset myopathy. Neuromuscul Disord 2006;16:427–31
15. Berciano J, Gallardo E, Dominguez-Perles R, et al. Autosomal dominant distal myopathy with a myotilin S55F mutation: Sorting out the phenotype. J Neurol Neurosurg Psychiatry 2008;79:205–8

16. Schröder R, Reimann J, Salmikangas P. et al. Beyond LGMD1A: Myotilin is a component of central core lesions and nemaline rods. Neuromuscul Disord 2003;13:451–55
17. Matsumoto H, Hayashi YK, Kim DS, et al. Congenital muscular dystrophy with glycosylation defects of alpha-dystroglycan in Japan. Neuromuscul Disord 2005;15:342–48
18. Starcevic M, Dell'Angelica EC. Identification of snapin and three novel proteins (BLOS1 BLOS2, and BLOS3/reduced pigmentation) as subunits of biogenesis of lysosome-related organelles complex-1 (BLOC-1). J Biol Chem 2004;279:28393–401
19. Falcon-Perez JM, Starcevic M, Gautam R, Dell'Angelica EC. BLOC-1, a novel complex containing the pallidin and muted proteins involved in the biogenesis of melanosomes and platelet-dense granules. J Biol Chem 2002;277:28191–99
20. Mitsuhashi H, Futa E, Sasagawa N, et al. Csk-homologous kinase interacts with SHPS-1 and enhances neurite outgrowth of PC12 cells. J Neurochem 2008;105:101–12
21. Selcen D. Myofibrillar myopathies. Curr Opin Neurol 2008;21:585–99
22. Vaughan KT, Weber FE, Einheber S, et al. Molecular cloning of chicken myosin-binding protein (MyBP) H (86-kDa protein) reveals extensive homology with MyBP-C (C-protein) with conserved immunoglobulin C2 and fibronectin type III motifs. J Biol Chem 1993;268:3670–76
23. Fucini P, Renner C, Herberhold C, et al. The repeating segments of the F-actin cross-linking gelation factor (ABP-120) have an immunoglobulin-like fold. Nat Struct Biol 1997;4:223–30
24. Barrachina M, Moreno J, Juves S, et al. Target genes of neuron restrictive silencer factor are abnormally up-regulated in human myotilinopathy. Am J Pathol 2007;171:1312–23

[Autophagy 5:6, 795-804; 16 August 2009]; ©2009 Landes Bioscience

Research Paper

Autophagic degradation of nuclear components in mammalian cells

Young-Eun Park,[1,2] Yukiko K. Hayashi,[1] * Gisèle Bonne,[3,4] Takuro Arimura,[5] Satoru Noguchi,[1] Ikuya Nonaka[1] and Ichizo Nishino[1]

[1]Department of Neuromuscular Research; National Institute of Neuroscience; National Center of Neurology and Psychiatry (NCNP); Kodaira, Tokyo Japan; [2]Department of Neurology and Medical Research Institute; Pusan National University Hospital; Seo-gu, Busan Korea; [3]Inserm-UPMC-CNRS UMRS_974; Institut de Myologie Paris, France; [4]AP-HP; Groupe Hospitalier Pitié-Salpêtrière, U.F. Cardiogénétique et Myogénétique; Service de Biochimie Métabolique; Paris, France; [5]Department of Molecular Pathogenesis; Medical Research Institute; Tokyo Medical and Dental University; Tokyo, Japan

Abbreviations: DAPI, 4',6-diamidino-2-phenylindole; GFP, green fluorescent protein; LC3, microtubule-associated protein 1 light chain 3; LC3-I, unlipidated form of LC3; LC3-II, lipidated form of LC3 (LC3-phopholipid conjugate); PI3K, phosphatidylinositol 3 kinase

Key words: autophagy, nuclear envelopathies, A-type lamins, emerin, nucleus

Autophagy is an evolutionarily conserved intracellular mechanism for the degradation of organelles and proteins. Here we demonstrate the presence of perinuclear autophagosomes/autolysosomes containing nuclear components in nuclear envelopathies caused by mutations in the genes encoding A-type lamins (*LMNA*) and emerin (*EMD*). These autophagosomes/autolysosomes were sometimes bigger than a nucleus. The autophagic nature is further supported by upregulation of LC3-II in *Lmna*$^{H222P/H222P}$ fibroblasts. In addition, inhibition of autophagy led to the accumulation of nuclear abnormalities and reduced cell viability, strongly suggesting a beneficial role of autophagy, at least in these cells. Similar giant autophagosomes/autolysosomes were seen even in wild-type cells, albeit rarely, implying that this "nucleophagy" is not confined to the diseased condition, but may be seen even in physiologic conditions to clean up nuclear wastes produced by nuclear damage.

Introduction

Nuclear envelopathies refer to disorders caused by mutations in the genes encoding nuclear envelope proteins, such as A-type lamins (*LMNA*) and emerin (*EMD*). *LMNA* mutations are known to cause a hererogeneous group of disorders collectively called as laminopathies, which encompass autosomal dominant and recessive forms of Emery-Dreifuss muscular dystrophy (AD and AR-EDMD), limb girdle muscular dystrophy type 1B (LGMD1B), cardiomyopathy with conduction defects, partial lipodystrophy, Charcot-Marie-Tooth disease type 2 and premature aging syndrome.[1-3] *EMD* mutations are causative for emerinopathies, a group of disorders that include X-linked EDMD, LGMD, cardiomyopathy with conduction defects, and familial atrial fibrillation.[4-6]

Because lamins form a protein meshwork of nuclear lamina at the nucleoplasmic side of inner nuclear membrane and have an important role in the maintenance of nuclear architecture, mutations in *LMNA* are thought to cause nuclear membrane fragility. This phenomenon is expected especially in skeletal and cardiac muscle cells which are constantly subjected to repeated mechanical stress. Loss of A-type lamins has been implicated to impair nuclear mechanics and increase nuclear fragility.[7-9] Loss of emerin, an inner nuclear membrane protein, could also lead to structural instability of nuclear membrane; emerin binds to several structural proteins in nucleus such as lamins, nesprins and nuclear actin, and can promote actin polymerization in vitro.[10-19]

In skeletal and cardiac muscles from patients with laminopathy and emerinopathy, various nuclear abnormalities have been observed, which are mainly composed of alteration in nuclear shape and emphasizing the role of lamins in the maintenance of nuclear integrity.[20-24] We recently demonstrated the presence of unique perinuclear vacuolar structures in the skeletal and/or cardiac muscles from laminopathy patients and emerin-null mice under electron microscopy,[21,25] but neither the nature of these structures nor their role in disease pathomechanism has ever been clarified. As most of these vacuolar structures contained amorphous and electron-dense materials resembling myelinated materials, we suspected that these are actually autophagic in nature.

Macroautophagy is a well-conserved molecular mechanism for the bulk degradation of organelles and proteins.[26-28] During autophagic process a double-membraned structure, the so-called phagophore or preautophagosome, randomly engulfs cytosolic components and cellular organelles. It is enclosed to form the so-called autophagosome, which is then fused with lysosome, enabling intra-autophagosomal components to be degraded by lysosomal hydrolases.[28]

Recently it has been alluded to that the autophagic process is also responsible for selective degradation of specific cellular

*Correspondence to: Yukiko K. Hayashi; National Institute of Neuroscience, NCNP; 4-1-1 Ogawa-Higashi; Kodaira, Tokyo 187-8502 Japan; Tel. 81.42.341.2711 Ex. 5113; Fax: 81.42.346.1742; Email: hayasi_y@ncnp.go.jp

Submitted: 11/17/08; Revised: 04/20/09; Accepted: 04/30/09

Previously published online as an *Autophagy* E-publication:
http://www.landesbioscience.com/journals/autophagy/article/8901

components; for instance, pexophagy works to decrease the number of peroxisome adapting to environmental changes in yeast, while mitophagy and ER-phagy have been suggested to degrade damaged mitochondria and overstressed endoplasmic reticulum, respectively.[29-31]

In this study, we show that the perinuclear vacuolar structures are actually giant autophagosomes/autolysosomes involved in the degradation of damaged nuclear components, extending the concept of macroautophagy in various cellular organelles to include the nucleus.

Results

Perinuclear vacuolar structures observed in skeletal and cardiac muscles of human and mouse nuclear envelopathy. Electron microscopic observation of skeletal muscles from patients with laminopathy revealed perinuclear vacuolar structures in ~10% of myonuclei.[21] Most of these structures were consistently found in close proximity to the irregularly-shaped nuclei which also contained disorganized chromatin structures. These vacuolar structures varied in size from 1.5 to 5 μm in diameter, and were observed to contain either diffuse granular, honeycomb-like or dense amorphous materials within multiple layered and folded membranes (Fig. 1A and B). Similar structures were also observed near the nuclei of nonmuscle cells from muscle specimens (Fig. 1C).

Perinuclear vacuolar structures were also detected in skeletal and cardiac muscles from different mouse models of nuclear envelopathies including emerin lacking *Emd*$^{-/-}$ (89 weeks of age),[15] A-type lamin-deficient *Lmna*$^{-/-}$ (10 weeks), and homozygous knock in *Lmna*$^{H222P/H222P}$ (24 weeks) mouse models (Fig. S1), and also in skin fibroblasts from 10-week-old *Lmna*$^{H222P/H222P}$ mouse (Fig. 1D).

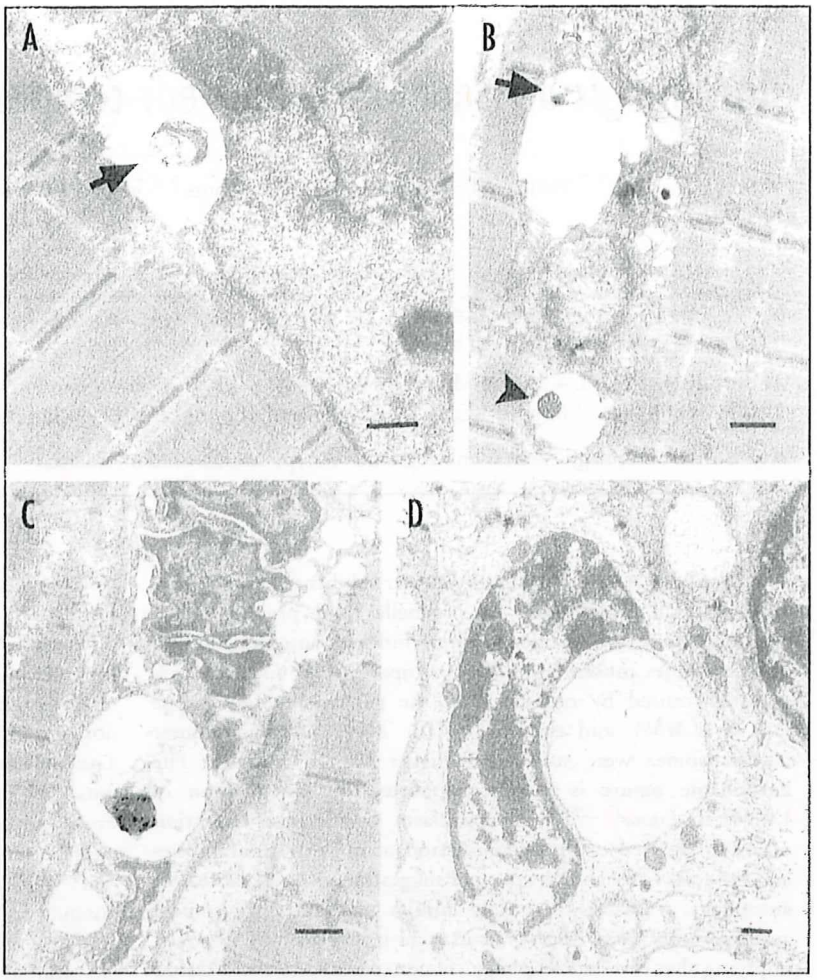

Figure 1. Electron microscopic observation of perinuclear vacuolar structures in skeletal muscles from patients (A–C) and skin from *Lmna*$^{H222P/H222P}$ mouse (D). (A–C) Perinuclear vacuolar structures of variable diameter usually contain myelinated (arrows) and dense amorphous materials (arrowhead) in muscle (A and B) and nonmuscle cells in skeletal muscle specimens (C) of patients with AD-EDMD/LGMD1B. (D) In the skin obtained from 10-week-old *Lmna*$^{H222P/H222P}$ mouse, similar perinuclear vacuolar structures are observed. Bars, 0.5 μm.

Electron microscopic observation of *Lmna*$^{H222P/H222P}$ MEF. For further characterization of nuclear changes, we used mouse embryonic fibroblasts (MEF) obtained from *Lmna*$^{H222P/H222P}$ mice. In these cells, nuclei had markedly irregular shape and in addition small particles with similar electron density to nucleus were seen (Fig. 2A, arrow). In some areas, there was blurring of the nuclear membrane, probably suggesting the disruption of nuclear membrane, where small circular structures were accumulated (Fig. 2A, arrowheads). Vacuolar structures from 3 to 7 μm in diameter were frequently found in the cytoplasm, especially near the blurred nuclear membrane, and appeared to fuse with one another (Fig. 2B). These vacuolar structures were mostly single- or double-membraned although in some cases it was difficult to recognize clear membranous structures (Fig. 2B and C). Smaller electron-dense vesicles were also much increased over the cytoplasm but more highlighted around large vacuolar structures (Fig. 2C and D). The contents of vacuolar structures were variable from granular substances to pieces of amorphous materials, but a few were empty (Fig. 2E–H).

Nuclear shape of cultured *Lmna*$^{H222P/H222P}$ MEF. To characterize perinuclear vacuolar structures by in vitro analysis, we performed immunocytochemistry on *Lmna*$^{H222P/H222P}$ MEF using antibodies against nuclear envelope proteins (e.g. lamins A, C and B, emerin and LAP2). The nuclei had markedly irregular shape and, in addition, single or multiple blebs and nuclear herniation were seen in 21 ± 1.8% of *Lmna*$^{H222P/H222P}$ cells (Fig. S2), similar to previous reports on fibroblasts from patients with *LMNA* mutations.[32,33] Nuclear envelope proteins were intensely stained at bleb sites (Fig. S2, arrowheads). Moreover, various-sized DAPI positive particles were often identified in the cytoplasm around nuclei

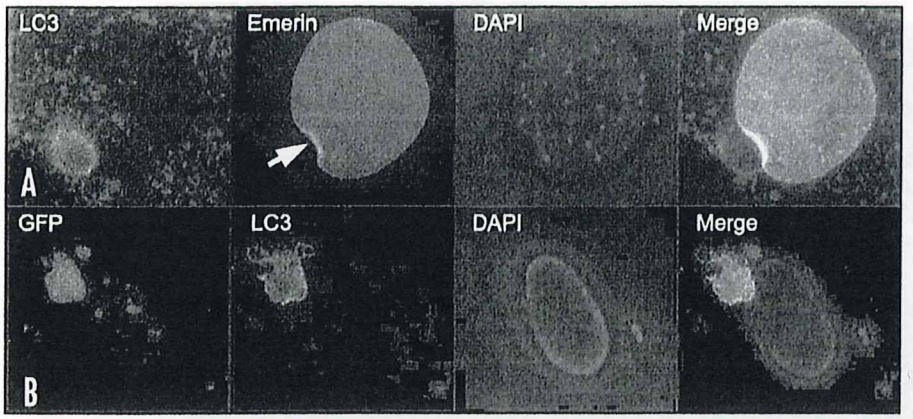

Figure 2. Electron microscopic findings of perinuclear vacuolar structures in *Lmna*$^{H222P/H222P}$ MEF. (A) A particle with similar electron density to the nucleus is detected near the nucleus (arrow). A part of nuclear membrane is blurred suggesting the disruption of nuclear membrane, where small circular structures are present (arrowheads). Vacuolar structures are identified near the nucleus, especially around the ruptured nuclear membrane. (B–D) Some cells contained multiple double- or single-membraned vacuolar structures together with electron dense smaller vesicles. (E–H) The contents of vacuolar structures are variable showing granular substances that fills the whole vacuole, or pieces of amorphous particles. A few are empty. Bars, 0.5 μm.

(Fig. S2, arrows). On the other hand, most of the wild-type cells displayed clearly round shape of nuclei, small blebs were identified only in less than 1% of the cells, and DAPI-positive particles were rarely seen outside nuclei.

Round-shaped LC3-positive signals close to the nuclei in *Lmna*$^{H222P/H222P}$ MEF. As we have insinuated that the vacuolar structures near the nuclei observed under electron microscope could be autophagic in nature, we performed immunocytochemical analysis of microtubule-associated protein 1/light chain 3 (LC3) in *Lmna*$^{H222P/H222P}$ fibroblasts. LC3 is a homologue of yeast Atg8 and is commonly used as a marker of autophagy because it decorates inner and outer membranes of autophagosome.[36] In about 10% of *Lmna*$^{H222P/H222P}$ cells, characteristically round LC3-positive signals were detected near or attached to the nucleus. The part of nuclear membrane interfacing with LC3-staining was sometimes strongly stained with lamin A and emerin (Fig. 3A, arrow). Similar findings were also observed in *Lmna*$^{-/-}$ fibroblasts.

Large-sized, round-shaped GFP staining close to nuclei in *Lmna*$^{H222P/H222P}$*/GFP-LC3* MEF. To further characterize the autophagic nature of these perinuclear structures, we produced *Lmna*$^{H222P/H222P}$*/GFP-LC3* transgenic mice. Green fluorescent protein-tagged-LC3 (GFP-LC3) transgenic mouse model has been developed for in vivo analysis of autophagy.[35] On immunocytochemistry, MEF from *Lmna*$^{H222P/H222P}$*/GFP-LC3* mice showed similar frequency of abnormally shaped nuclei to *Lmna*$^{H222P/H222P}$ cells. In addition, perinuclear round GFP-positive staining, sometimes bigger than the nuclei, were detected in about 10% of observed cells whereas it was rarely seen in wild-type/*GFP-LC3* cells under similar standard culture condition. In addition, these GFP-positive perinuclear signals were almost completely colocalized with LC3 in *Lmna*$^{H222P/H222P}$*/GFP-LC3* cells (Fig. 3B), being diffusely distributed over or outlining GFP signal.

As the activation of autophagy is induced by the upregulation of certain molecules, we examined the expression of other known autophagy-related proteins in *Lmna*$^{H222P/H222P}$*/GFP-LC3* fibroblasts to know whether similar machinery to macroautophagy is working in these cells. In a considerable number of cells, the perinuclear GFP-positive signals colocalized with Atg5 and Atg16L (Fig. 4A), which are known to participate in the initiation of phagophore (or preautophagosome) formation in mammalian cells.[36] Along the border of the perinuclear GFP-positive signals, we observed positive immunoreaction to Atg9 (Fig. 4B), which is associated with phagophore expansion.[37] The GFP signals also colocalized with Rab7 (Fig. 4C), which is known as a small GTPase protein associated with autophagosome maturation.[38] We also checked the involvement of lysosomes, and found that LAMP2, a lysosomal membrane protein, was identified around and inside GFP-positive staining (Fig. 4D); this finding was confirmed by the colocalization of GFP signals with Lyso-Tracker[®] which marks lysosome (Fig. 4E). With these findings, we can consider that the large perinuclear GFP signals are giant autophagosomes/autolysosomes.

Intriguingly, GFP-positive autophagosomes/autolysosomes contained extranuclear DAPI with variable staining intensity from intense to blurred or faint (Figs. 3–5). These DAPI signals were colocalized with histone H1 (Fig. 5A), but were rarely co-stained with nuclear envelope proteins such as lamin A and B (Fig. 5B and C), indicating that these are actually extranuclear and may indicate damaged DNA. We therefore immunostained with anti-γH2AX, a marker of DNA double-strand breaks caused by various insults which is known to have certain roles in the recognition and repair of damaged DNA.[39] Some of the extranuclear DAPI signal was colocalized with γH2AX and contained in GFP-positive autophagosomes/autolysosomes (Fig. 5D, arrowhead). γH2AX was detected also in intranuclear portions, mainly in blebbings (data not shown). These results suggest that extranuclear damaged DNA is destined for autophagic degradation. On the other hand, we could not find any overlap staining of LC3 and DAPI in rarely observed markedly fragmented nuclei with γH2AX staining, although LC3-positive signals can be seen in the cytoplasm (Fig. 5E).

Notably, in wild-type/*GFP-LC3* cells, similar autophagosomes/autolysosomes containing extranuclear DAPI signals were likewise observed, but with rare frequency of less than 0.1%.

Both LC3-II protein amount and transcriptional level of Maplc3b were increased in *Lmna*$^{H222P/H222P}$ MEF. On immunoblotting analysis, the protein amount of LC3-II, which is a lipidated form of LC3 and a marker of autophagosome formation, was significantly increased in *Lmna*$^{H222P/H222P}$ compared

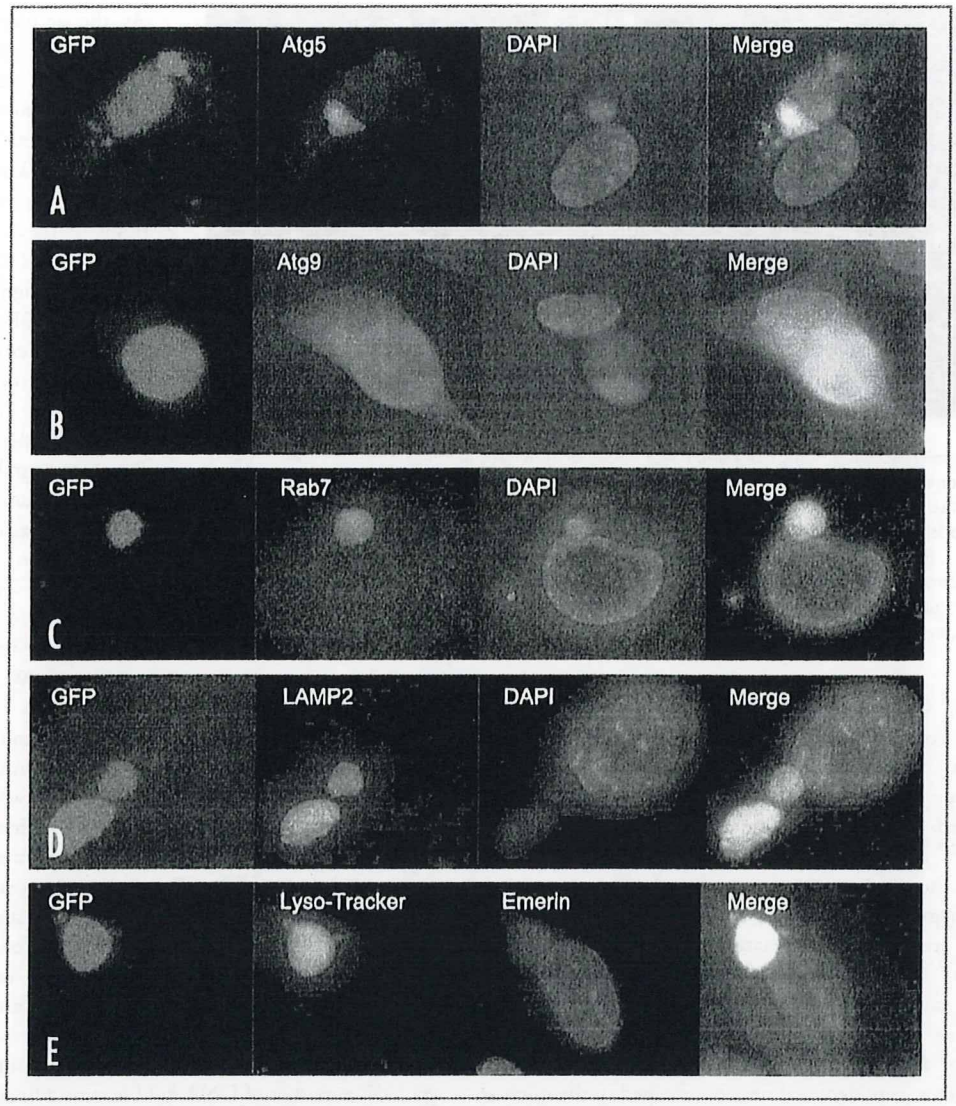

Figure 3. Perinuclear LC3 staining in *Lmna*$^{H222P/H222P}$ and *Lmna*$^{H222P/H222P}$/*GFP-LC3* MEFs. (A) In *Lmna*$^{H222P/H222P}$ MEF, a large-sized and round-shaped LC3-positive vacuolar structure is seen with stronger marginal dot-like staining. DAPI-positive materials are included within. Emerin is more strongly stained in the part of nuclear membrane interfacing with the LC3-positive structures (arrow). (B) In *Lmna*$^{H222P/H222P}$/*GFP-LC3* MEF, LC3 signal is detected with the GFP.

with wild-type cells (Fig. 6A). Because an increased amount of LC3-II could be interpreted either as increased autophagy influx or blocked autophagosome maturation,[40] we quantified the amount of LC3-II with or without lysosomal protease inhibitors (pepstatin A and E64d). LC3-II in *Lmna*$^{H222P/H222P}$ cells was much increased with lysosomal inhibitors (Fig. 6A), implying that the increased LC3-II amount is due to enhanced autophagy influx and not due to impedance of autophagosome maturation.

This increase in LC3-II protein might be also due to transcriptional upregulation of *Maplc3b* encoding a major form of LC3. By quantitative real-time PCR of *Maplc3b*, we observed that the transcriptional level of LC3 was significantly higher in *Lmna*$^{H222P/H222P}$ compared with wild-type MEF (Fig. 6B, $p = 0.0141$); relative copy number of LC3 mRNA in *Lmna*$^{H222P/H222P}$ MEF was 1.36 times when standardized by G3PDH transcriptional level.

Inhibition of autophagy increased the frequency of nuclear abnormalities and decreased cell viability in *Lmna*$^{H222P/H222P}$ MEF. To elucidate the role of autophagy in *Lmna*$^{H222P/H222P}$ cells, we inhibited autophagy by using 3-methyladenine (3-MA) and wortmannin. Autophagy was efficiently inhibited as the amount of LC3-II was notably decreased both in wild-type and *Lmna*$^{H222P/H222P}$ cells (Fig. 7A).

The number of LC3-positive autophagosomes was significantly decreased in the treated *Lmna*$^{H222P/H222P}$ cells compared with the untreated cells (Fig. 7B, $p < 0.0001$). Moreover, LC3 staining was

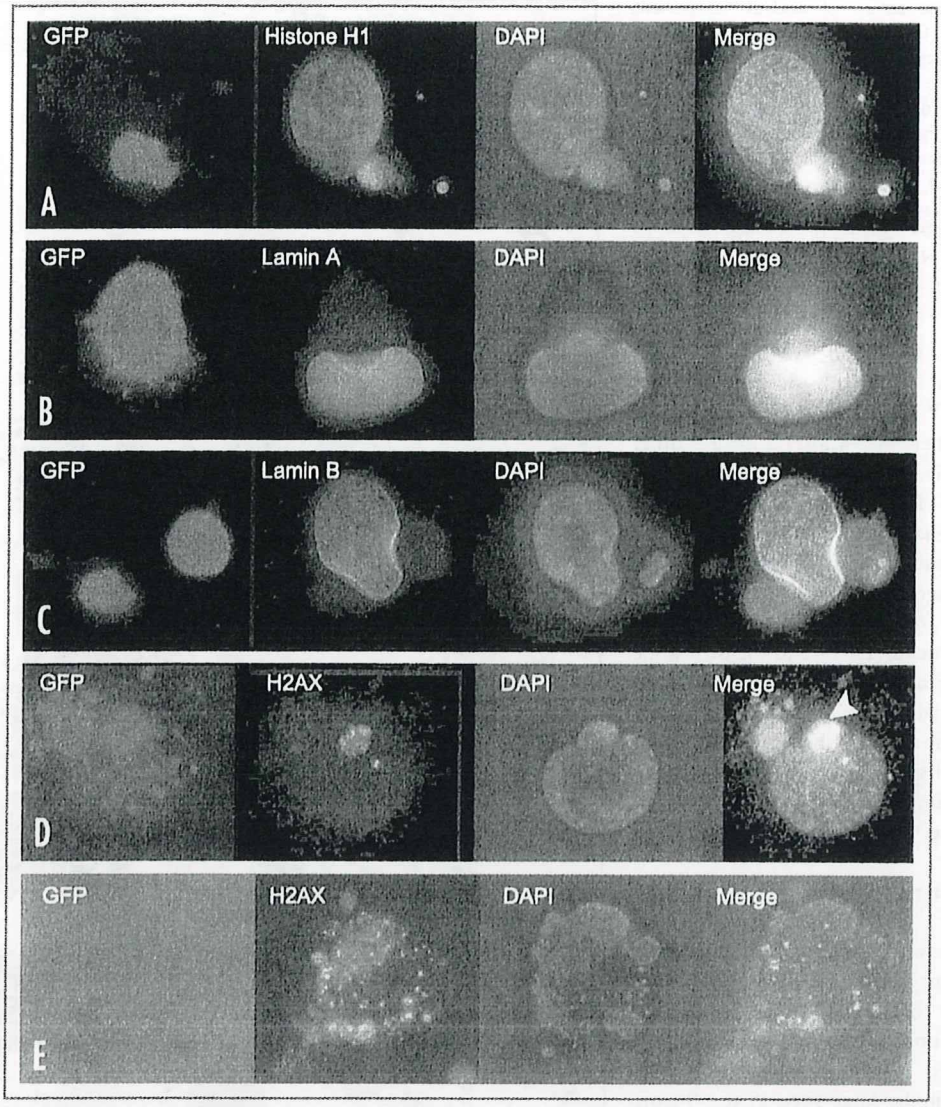

Figure 4. Involvement of autophagy-related proteins and LAMP2, and Lyso-Tracker® probe staining in *Lmna*$^{H222P/H222P}$/GFP-LC3 MEF. Atg5 (A), Atg9 (B), Rab7 (C) and LAMP2 (D) are all remarkably stained in/around the GFP-positive structures. (E) Lyso-Tracker® is highlighted and localized with the GFP-positive structures near nucleus.

virtually absent in the treated cells, even in nuclei with markedly irregular shape and with extranuclear DAPI signals, whereas it was often presented in untreated cells (Fig. 7C, upper). In addition, the number of cells with markedly irregular nuclei and/or extranuclear DAPI, as represented in Figure 7C, was much increased when autophagy was inhibited: the percentage of cells with nuclear deformation was 6.7 ± 1.2 and 9.8 ± 1.6 (mean ± SD), and cells with single or multiple extranuclear DAPI was 8.3 ± 0.9 and 14.9 ± 1.5 in untreated and treated cells, respectively (Fig. 7D). The difference between the two groups was statistically significant ($p = 0.0008$) after treatment.

We also checked mean survival rate by staining viable and dead cells in untreated wild-type (0.88), treated wild-type (0.83), untreated *Lmna*$^{H222P/H222P}$ (0.87) and treated *Lmna*$^{H222P/H222P}$ (0.72) cells (Fig. 7E). When autophagy was inhibited, the survival rate of *Lmna*$^{H222P/H222P}$ cells was significantly decreased ($p = 0.0029$) as compared to wild-type cells. This result implies that autophagy could have a beneficial effect on cell survival.

Discussion

Here we provide evidence that a part of the nucleus is degraded by autophagy when nuclei are damaged and/or partially extruded into the cytoplasm as frequently observed in nuclear envelopathy.

In *Lmna*$^{H222P/H222P}$/GFP-LC3 MEF, GFP-positive signals were presented near nuclei, which were proved to be identical to LC3-positive autophagosomes. The difference in staining

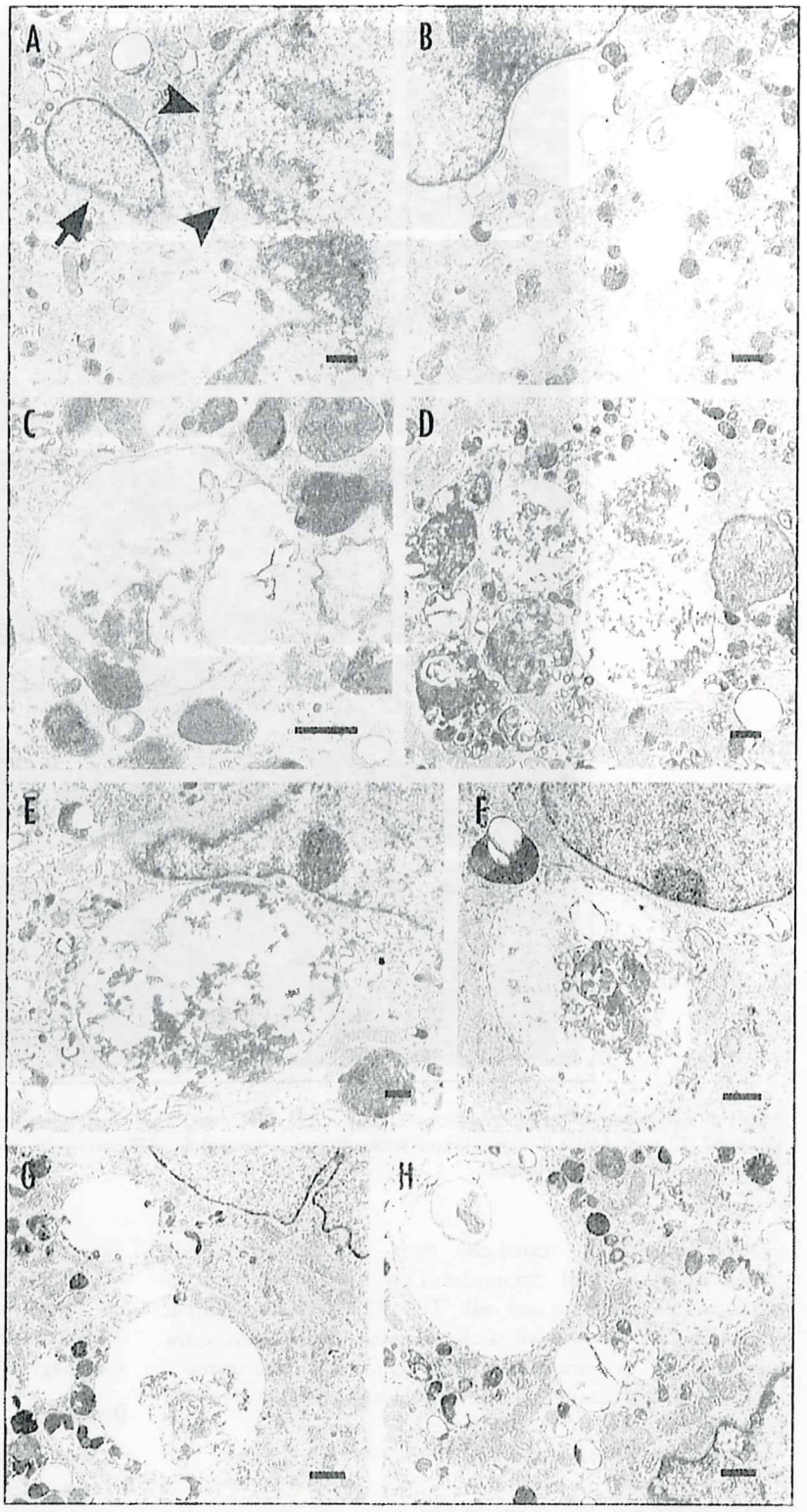

Figure 5. Characterization of nuclear components contained in the GFP-positive autophagosomes on immunocytochemistry. (A–C) GFP-positive autophagosomes with variable sized are seen close to the nuclei, and most of which are partially colocalized with DAPI signals outside of nucleus. Extranuclear DAPI signals in the GFP-positive autophagosomes are positive for histone H1 (A), but not for nuclear envelope proteins such as lamin A and B (B and C). (D) Extranuclear DAPI signals with GFP staining are positive for γH2AX (arrowhead). (E) Nuclear fragments with scattered γH2AX staining are negative for LC3.

pattern between GFP and LC3 despite their essential identity is probably due to the accumulation of GFP that is resistant to lysosomal hydrolase. Further immunostaining of other autophagy-related proteins (i.e., Atg5, 16L, 9 and Rab7) and LAMP2 confirmed that the GFP-positive signals are ultimately autophagosomes and autolysosomes. Our findings indicate that the autophagosomes appear to degrade the extruded nuclear components since most of them contained extranuclear DAPI and major histone protein H1 within. Irregularly blurred or faint DAPI or H1 signals inside the autophagosomes/autolysosomes substantiate that nuclear components are being degraded by autophagic process. The target of autophagy is probably the damaged portions of nuclei as demonstrated by γH2AX immunostaining.

Electron microscopic observations of *Lmna*$^{H222P/H222P}$ cells demonstrated that autophagosomes were clustered and lysosomes fused to form giant autophagosomes, which were sometimes bigger than nuclei. Giant autophagosomes are quite unusual and are rarely seen in starvation-induced autophagy, where the size is about 1 μm.[35] Similar large-sized (5 to 10 μm) autophagosomes has been reported to encircle bacteria in HeLa cells under group A streptococcus infection although the mechanism to form such giant autophagosomes was not clarified.[41] From our findings it can be suggested that the formation of giant autophagosomes may be required for the degradation of large molecules, such as a part of nucleus.

We propose that *Lmna*$^{H222P/H222P}$ nuclei, having incomplete lamina structure and frequently subjected to mechanical stress, subsequently become damaged and would apparently require (giant) autophagosome for degradation by lysosomal enzymes. Thus, it seems that this nuclear autophagy is consistent with macroautophagy in terms of its morphology and machinery used. On the other hand, piecemeal microautophagy of nucleus (PMN) has been recently

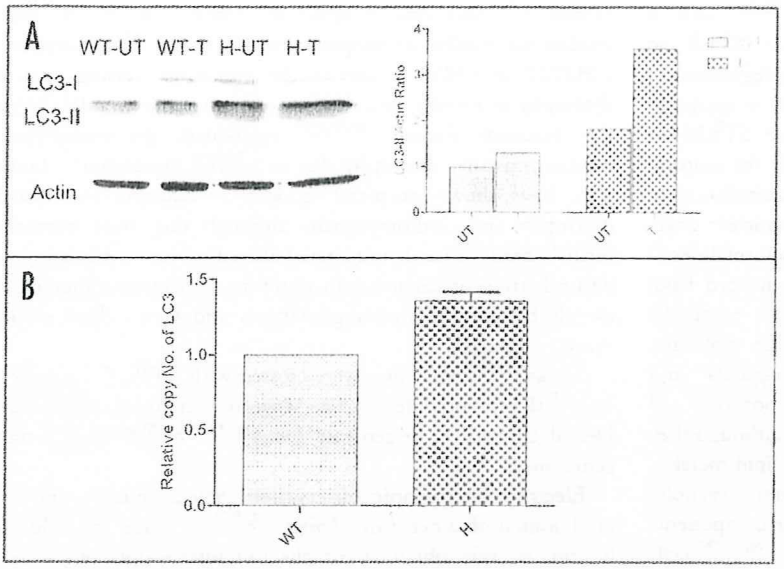

Figure 6. Immunoblotting analysis of LC3 and quantitative real-time PCR of *Maplc3b*. (A) The amount of LC3-II is highly increased in *Lmna*$^{H222P/H222P}$ cells, and which gets more increased with the treatment of lysosomal protease inhibitors (pepstatin A and E64d), suggesting that autophagy is markedly activated in the diseased cells. (B) By quantitative real-time PCR of *Maplc3b*, the transcriptional level of LC3 is represented to be significantly increased in *Lmna*$^{H222P/H222P}$ MEF compared with wild-type ($p = 0.0141$). WT-UT, untreated wild-type; WT-T, treated wild-type; H-UT, untreated *Lmna*$^{H222P/H222P}$; H-T, treated *Lmna*$^{H222P/H222P}$ cells.

reported in *S. cerevisiae*, which is induced by nutritional depletion or rapamycin stimulation. During PMN, velcro-like patches are formed by the interaction between nuclear membrane and outer nuclear membrane at nonessential portions of nuclei. PMN is morphologically categorized as microautophagy because nuclear components are directly engulfed by vacuoles without formation of vesicular intermediates, i.e. autophagosomes.[] This concept was further supported by a recent investigation that elucidated the core machinery of PMN.[] Because detailed underlying molecular mechanism is still unclear, we could not completely exclude the possible involvement of microautophagy for degradation of nuclear blebs observed in *Lmna*$^{H222P/H222P}$ cells.

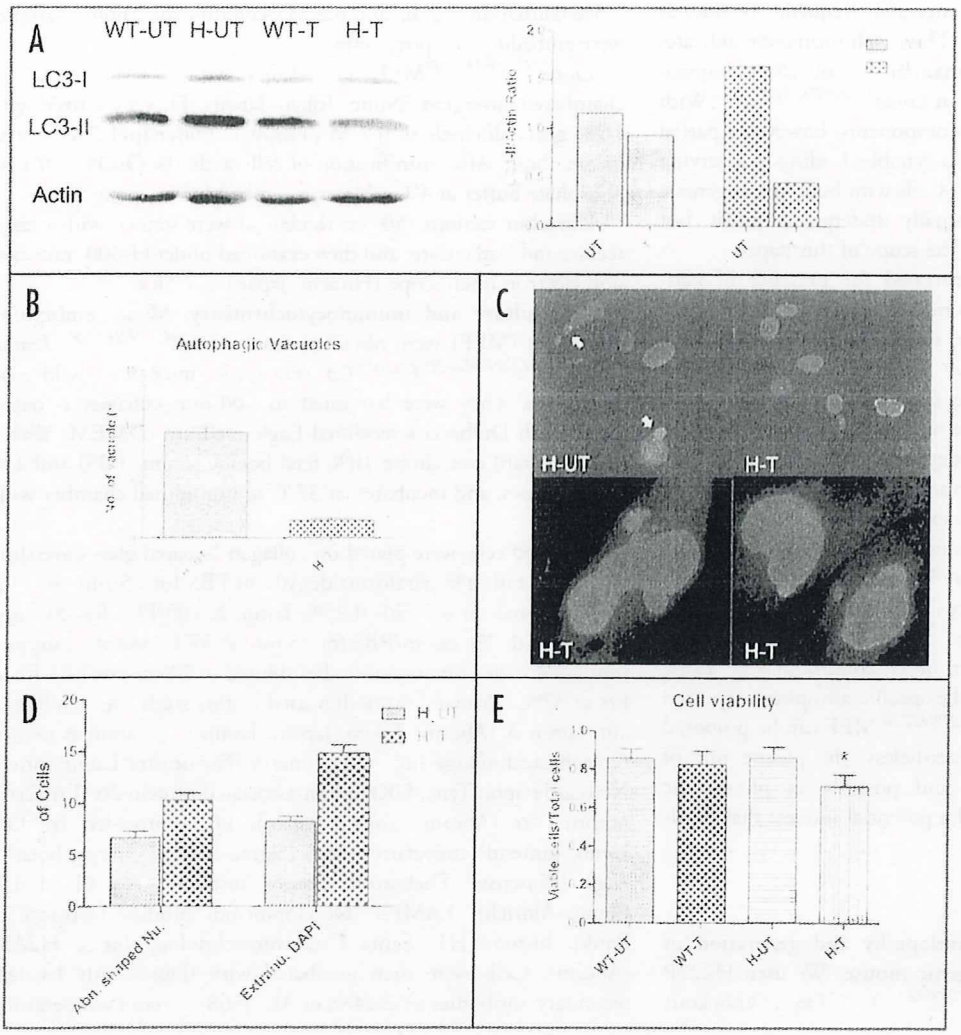

Figure 7. Changes in nuclear abnormalities and cell survival rate after autophagy inhibition. (A) Immunoblotting analysis of LC3 shows that LC3-II is decreased after autophagy inhibition in wild-type and *Lmna*$^{H222P/H222P}$ cells. (B) In treated *Lmna*$^{H222P/H222P}$ cells, autophagic vacuoles are significantly decreased compared with untreated cell ($p = 0.0001$). (C) On immunocytochemistry of LC3 (red), lamin C (green) and DAPI (blue), the treated *Lmna*$^{H222P/H222P}$ cells rarely show LC3 staining whereas untreated cells frequently display perinuclear autophagosomes (arrows, upper). With autophagy inhibition, cells present severe deformation of nuclei and multiple extranuclear DAPI (lower). (D) The number of cells with markedly irregular shaped nuclei and extranuclear DAPI is much increased by autophagy inhibition ($p = 0.0008$). (E) Cell viability assay represents the decreased cell survival rate in *Lmna*$^{H222P/H222P}$ cells by autophagy inhibition compared with wild-type cells (*$p = 0.0029$). WT, wild-type; H, *Lmna*$^{H222P/H222P}$; UT, untreated; T, treated.

The activation of autophagy in *Lmna*$^{H222P/H222P}$ cells is supported by the finding of increased amount of LC3-II on immunoblotting analysis, and the transcriptional upregulation of LC3 expression. LC3 has been previously reported to be increased in progeroid mice lacking zinc metalloproteinase STE24 or ZMPSTE24 (*Zmpste24*$^{-/-}$),[45] an enzyme required for the maturation of lamin A. ZMPSTE24 deficiency causes accumulation of the premature form of lamin A (prelamin A) in nuclear envelope and leads to profound nuclear architecture abnormalities.[46] Increased LC3 was thought to be secondary to enhanced basal autophagy in skeletal and cardiac muscles due to a metabolic derangement in progeroid mice. Considering similar molecular defects of nuclear lamina in two mouse models of *Zmpste24*$^{-/-}$ and *Lmna*$^{H222P/H222P}$, we cannot totally exclude the possibility of increased basal autophagy in *Lmna*$^{H222P/H222P}$ mice although they did not show comparable alterations in glucose and lipid metabolism.[47] In this study, the finding that GFP-LC3-positive vacuoles were consistently related to the cytoplasmic nuclear components could indicate that activated autophagy in *Lmna*$^{H222P/H222P}$ cells may at least in part be induced by the nuclear damage.

Reduced cell viability in *Lmna*$^{H222P/H222P}$ cells after autophagy inhibition probably resulted from increased frequency of nuclear abnormalities as shown in Figure 7. This result ultimately indicates that autophagy is working for the maintenance of cellular homeostasis by cleaning up nuclear wastes in *Lmna*$^{H222P/H222P}$ cells. With autophagic degradation of nuclear components, however, a partial loss of genetic information may be inevitable, leading to a varying degree of molecular defects on cells. Cells with bulk loss of genetic materials can be thought to eventually undergo apoptosis, but clarification of this issue is beyond the scope of this paper.

In conclusion, we have demonstrated the presence of perinuclear autophagosomes/autolysosomes in *Lmna*$^{H222P/H222P}$ cells. Notably, in the area of nuclear membrane interfacing with autophagosomes/autolysosomes, we could see accumulation of nuclear envelope proteins. This may suggest that autophagy could contribute to the rapid repair of the nuclear membrane, as there is a need to rescue the cells from overdegradation or to minimize the loss of nuclear components after nuclear membrane injury. This would be worth exploring in future experiments.

It is also notable that similar autophagosomes/autolysosomes containing nuclear components were found even in wild-type cells although to a much lower frequency. This implies that autophagic degradation of nuclear components is not confined to nuclear envelopathy, and can occur under other conditions that cause nuclear damage. Like other organelle-specific autophagy reported to date, the autophagy in *Lmna*$^{H222P/H222P}$ MEF can be proposed to be called as nucleophagy. Nevertheless, the precise role of 'nucleophagy' in laminopathies, and possibly in physiologic conditions, remains perplexing and a potential interest that needs to be elucidated.

Materials and Methods

Mouse models for nuclear envelopathy and generation of *Lmna*$^{H222P/H222P}$*/GFP-LC3* transgenic mouse. We used H222P homozygous knock-in (*Lmna*$^{H222P/H222P}$), *Lmna* knockout (*Lmna*$^{-/-}$)[48] and emerin knockout (*Emd*$^{-/-}$) mice[35] as mouse models for nuclear envelopathy in this study. The mutation of p.H222P in *LMNA* is one of the mutations causing muscular dystrophy in human, and the homozygous mouse model carrying the mutation, *Lmna*$^{H222P/H222P}$ reproduced the phenotype of human muscular dystrophy due to *LMNA* mutations.[47] *Lmna*$^{-/-}$ mice have shown postnatal lethality in addition to muscular dystrophy and cardiomyopathy although they were normal at birth.[48] *Emd*$^{-/-}$ mice demonstrated altered motor coordination and delayed atrioventricular conduction time in electrocardiogram, but overall they showed normal growth rate and were without obvious muscle weakness.

Lmna$^{H222P/H222P}$ mice were crossed with GFP-LC3 transgenic mice[35] (kindly provided by Dr. Mizushima in Tokyo Medical and Dental University) to generate *Lmna*$^{H222P/H222P}$*/GFP-LC3* transgenic mice.

Electron microscopic observation. Soleus muscles and skin of abdomen obtained from *Lmna*$^{H222P/H222P}$ mice and wild-type littermates were obtained for electron microscopic observation. Tissues were fixed with 3% glutaraldehyde in 0.1 M cacodylate buffer. After shaking with a mixture of 4% osmium tetroxide + 5% lanthanum nitrate and 0.2 M s-collidine for 2 hours, samples were embedded in epoxy resin.

Lmna$^{H222P/H222P}$ MEF were cultured and grown on Lab-Tek II chambered coverglass (Nunc, Tokyo, Japan). They were fixed with 1.2% glutaraldehyde in 0.1 M phosphate buffer (pH 7.4) at 4°C for one hour. After osmification of cells with 1% OsO_4 in 0.1 M phosphate buffer at 4°C, they were embedded in epoxy resin.

Ultrathin sections (50 nm thickness) were stained with uranyl acetate and lead citrate and then examined under H-600 transmission electron microscope (Hitachi, Japan) at 75 kV.

Cell culture and immunocytochemistry. Mouse embryonic fibroblasts (MEF) were obtained from *Lmna*$^{H222P/H222P}$, *Lmna*$^{-/-}$, *Lmna*$^{H222P/H222P}$*/GFP-LC3* transgenic mice and wild-type littermates. They were harvested in 100-mm collagen I-coated dishes with Dulbecco's modified Eagle medium (DMEM, Wako, Osaka, Japan) containing 10% fetal bovine serum (FBS) and 1% of antibiotics, and incubated at 37°C in humidified chamber with 5% CO_2.

Cultured cells were plated on collagen I-coated glass coverslips and fixed with 4% paraformaldehyde in PBS for 15 min at 4°C, permeabilized on ice with 0.25% Triton X-100/PBS for 20 min, blocked with 2% casein/PBS for 15 min at 37°C, and then immunostained with primary antibodies diluted in 2% casein/PBS for 2 hrs at 37°C. Primary antibodies used in this study are as follows: anti-lamin A (Abcam, Tokyo, Japan), lamin C, lamin B (Santa Cruz Biotechnology Inc., CA), emerin (Novocastra Laboratories, Newcastle upon Tyne, UK), lamin-associated protein 2α (LAP2α), nesprin 1α (Abcam, Tokyo, Japan), LC3 (provided by Dr. Ueno, Juntendo university), Atg5 (Sigma-Aldrich, Tokyo, Japan), Atg9 (Biosensis, Thebarton, South Australia), Atg16L, Rab7 (Sigma-Aldrich), LAMP2 (Developmental Studies Hybridoma Bank), histone H1 (Santa Cruz Biotechnology Inc.), H2AX (Abcam). Cells were then incubated with fluorescently labeled secondary antibodies (Alexa488 or Alexa568) at room temperature

for 45 min. Coverslips were mounted together with 4',6-diamidino-2-phenylindole (DAPI, Invitrogen, CA) for nuclear localization and then visualized under epifluorescence using Axiophoto II (Carl Zeiss).

To detect lysosomal localization, cells were incubated with PBS containing 100 nM of Lyso-Tracker® (Invitrogen) at 37°C for 1 hour. After rinsing with PBS, cells were fixed with 4% paraformaldehyde at 37°C for 20 min.

Immunoblotting analysis of LC3. *Lmna*$^{H222P/H222P}$ and wild-type MEF were grown on 100 mm-collagen I coated dishes. At 80% confluent state, cells were treated with lysosomal protease inhibitors consisting of pepstatin A (20 μg/mL, Peptide Institute, Osaka Japan) and E64d (20 μg/mL, Peptide Institute), or with dimethylsulfoxide (DMSO) as a negative control for 4 hours. Whole cell lysates was extracted with lysis buffer (1% NP-40 cell lysis buffer supplemented with protease inhibitor). Immunoblotting analysis of LC3 was performed according to the standard method. Twenty micrograms of protein of each sample were loaded on 12.5% sodium dodecyl sulfate-polyacrylamide gel. After electrophoresis, the gel was transferred to polyvinylidene (PVDF) membrane and immunostained with anti-LC3 antibody. Data was analyzed by using LAS-1000 chemiluminescence imaging system (Fujifilm, Tokyo, Japan).

Quantitative real-time PCR. Total RNA was extracted from *Lmna*$^{H222P/H222P}$ and wild-type MEF with TRIzol (Invitrogen) following manufacturer's protocol. Single stranded cDNA was synthesized from RNA using SuperScript™ III reverse transcriptase. Gene expression of LC3B was quantified by quantitative real-time PCR in Rotor-Gene™ 6000 system (Corbett Life Science, NSW, Australia), using the following primers: LC3b-F: CCG AGA AGA CCT TCA AGC AG and LC3b-R: CCA TTC ACC AGG AGG AAG AA. All the results were normalized with respect to G3PDH expression.

Autophagy inhibition. MEF from *Lmna*$^{H222P/H222P}$ mice and wild-type littermates were treated with 10 mM 3-MA (Sigma-Aldrich) and 200 nM wortmannin (Sigma-Aldrich), which are also known as phosphatidylinositol-3 kinase inhibitors and autophagy inhibitors, or negative control at 80% confluent state for 2 hours as previously described.[19] After the treatment, the amount of LC3 was measured by immunoblotting analysis. Immunocytochemistry of LC3 and a nuclear envelope protein (lamin C) was also performed to check the changes in nuclear abnormalities with autophagy inhibition. For the calculation of cell survival rate, the cells were stained by acetoxymethyl ester of calcein (Calcein-AM, Dojindo, MD) and propidium iodine (PI, Dojindo) for 15 min at 37°C according to the manufacturer's instruction. This staining method can differentiate green-colored viable and red-colored dead cells, respectively. Cell viability was determined as the ratio of the number of viable cells per total number of cells in four groups of untreated wild-type, treated wild-type, untreated *Lmna*$^{H222P/H222P}$ and treated *Lmna*$^{H222P/H222P}$ cells.

Statistical analyses. To get quantitative data, three to four replicates of measurement were done for each condition. All the data were presented as mean and standard deviation. Comparisons among groups were done by using student t test and analysis of variance (ANOVA) as appropriate. Statistical significance was considered when p value was less than 0.05.

Acknowledgements

We thank Drs. Colin L. Stewart (National Cancer Institute, MD, USA) and Dr. Noboru Mizushima (Tokyo Medical and Dental University, Tokyo) for providing mice of *Lmna*$^{-/-}$ and GFP-LC3, respectively, and Dr. May Christine V. Malicdan (National Institute of Neuroscience, NCNP) for reviewing the manuscript. This study was supported by the "Research on Psychiatric and Neurological Diseases and Mental Health" of "Health Labour Sciences Research Grant" and the "Research Grant (20B-12, 20B-13) for Nervous and Mental Disorders" from the Ministry of Health, Labor and Welfare; Human Frontier Science Program; Grant-in-Aid for Scientific Research from Japan Society for the Promotion of Science; Research on Publicly Essential Drugs and Medical Devices from the Japanese Health Sciences Foundation; and Program for Promotion of Fundamental Studies in Health Sciences of the National Institute of Biomedical Innovation (NIBIO).

Note

Supplementary materials can be found at: www.landesbioscience.com/supplement/ParkAUTO5-6-Sup.pdf

References

1. Bonne G, Di [illegible] MR, [illegible] S, Bec[illegible] HJ, [illegible] Merlin [illegible] al. Mutations in the [illegible] encoding lamin A/C cause [illegible] dominant [illegible] muscular dystrophy. Nat Genet 1999; [illegible]
2. Raffaele Di Barletta M, [illegible] E, [illegible] Toniolo D, [illegible] et al. Different mutations in the LMNA gene cause autosomal dominant and autosomal recessive Emery-Dreifuss muscular dystrophy. Am J Hum Genet 2000; 66:1407-[illegible]
3. Muchir A, Bonne G, [illegible] van der Kooi AJ, van Meegen M, Baas F, Bolhuis [illegible] Identification of mutations in the gene encoding lamins A/C in autosomal dominant limb girdle muscular dystrophy with atrioventricular conduction disturbances (LGMD1B). Hum Mol Genet 2000; 9:1453-[illegible]
4. Fatkin D, MacRae C, Sasaki T, Wolff MR, Porcu [illegible] Frenneaux M, et al. Missense mutations in the rod domain of the lamin A/C gene as causes of dilated cardiomyopathy and conduction-system disease. N Engl J Med 1999; [illegible]
5. Becane HM, Bonne G, Varnous S, Muchir A, [illegible] Hammouda [illegible] et al. High incidence of sudden death with conduction system and myocardial disease due to lamins A and C gene mutation. Pacing Clin Electrophysiol 2000; [illegible] 1661-[illegible]
6. [illegible] Nuclear lamin A/C R482Q mutation in canadian Dunnigan-type familial partial lipodystrophy. Hum Mol Genet 2000; [illegible] 109-12.
7. De Sandre-Giovannoli A, Chaouch M, Kozlov S, Vallat JM, Tazir M, Kassouri N, et al. Homozygous defects in LMNA, encoding lamin A/C nuclear-envelope proteins, cause autosomal recessive axonal neuropathy in human (Charcot-Marie-Tooth disorder type 2) and mouse. Am J Hum Genet 2002; [illegible] 726-[illegible]
8. De Sandre-Giovannoli A, Bernard R, Cau P, Navarro C, Amiel J, Boccaccio [illegible] Lamin A truncation in Hutchinson-Gilford progeria. Science 2003; 300:2055.
9. Eriksson M, Brown WT, Gordon LB, [illegible] MW, [illegible] Scott [illegible] Recurrent de novo point mutations in lamin A cause Hutchinson-Gilford progeria syndrome. Nature 2003; 4[illegible] 293-8.
10. Bione S, Maestrini E, Rivella S, Mancini M, Regis S, Romeo G, Toniolo D. Identification of a novel X-linked gene responsible for Emery-Dreifuss muscular dystrophy. Nat Genet 1994; [illegible]
11. [illegible]ra S, Hayashi YK, [illegible] K, [illegible] MN, [illegible] Nagai [illegible] et al. [illegible] muscular dystrophy due to emerin gene mutations. Arch Neurol 2007; 6[illegible] 1038-[illegible]
12. [illegible] KL, [illegible] TM. X-linked [illegible] [illegible] by [illegible] J [illegible] 2007; [illegible]
13. [illegible] R, [illegible] A, Arimura T, [illegible] Ben Yaou R, Bonne G, [illegible] Molecular and [illegible] LMNA and EMD mutations: Role of [illegible] Neurology 2007; [illegible] 188; 9[illegible]
14. Broers JL, Peeters EA, Kuijpers HJ, [illegible] Bouten CV, [illegible] W, et al. Decreased mechanical stiffness in LMNA-/- cells is caused by defective nucleo-cytoskeletal integrity: implications for the development of laminopathies. Hum Mol Genet 2004; 13:2567-80.

15. Lammerding J, Schulze PC, Takahashi T, Kozlov S, Sullivan T, Kamm RD, et al. Lamin A/C deficiency causes defective nuclear mechanics and mechanotransduction. J Clin Invest 2004; [illegible]70-8.
16. Sakaki M, Koike H, Takahashi N, Sasagawa N, Tomioka S, Arahata K, Ishiura S. Interaction between emerin and nuclear lamins. J Biochem 2001; 129:321-7.
17. Mislow JM, Holaska JM, Kim MS, Lee KK, Segura-Totten M, Wilson KL, McNally EM. Nesprin-1alpha self-associates and binds directly to emerin and lamin A in vitro. FEBS Lett 2002; 525:135-40.
18. Bengtsson L, Wilson KL. Multiple and surprising new functions for emerin, a nuclear membrane protein. Curr Opin Cell Biol 2004; 16:73-9.
19. Zhang Q, Ragnauth CD, Skepper JN, Worth NF, Warren DT, Roberts RG, et al. Nesprin-2 [illegible] isomeric protein that binds lamin and emerin at the nuclear envelope and forms a subcellular network in skeletal muscle. J Cell Sci 2005; 118:673-87.
20. Sabatelli P, Lattanzi G, Ognibene A, Columbaro M, [illegible] C, Merlini L, et al. Nuclear alterations in autosomal-dominant Emery-Dreifuss muscular dystrophy. Muscle Nerve 2001; 24:826-9.
21. Park YE, Hayashi YK, Goto K, Nonaka I, Noguchi S, Nishino I. Nuclear Changes in Skeletal Muscle [illegible] AD-EDMD [illegible] Neuromuscul Disord 2008; In Press.
22. Fidzianska A, Toniolo D, Hausmanowa-Petrusewicz I. Ultrastructural abnormality of sarcolemmal nuclei in Emery-Dreifuss muscular dystrophy (EDMD). J Neurol Sci 1998; 159:88-93.
23. Fidzianska A, Hausmanowa-Petrusewicz I. Architectural abnormalities in muscle nuclei. Ultrastructural differences between X-linked and autosomal dominant forms of EDMD. J Neurol Sci 2003; [illegible]:47-51.
24. Fidzianska A, Bilinska ZT, Tesson F, Wagner T, Walski M, Grzybowski J, et al. Obliteration of cardiomyocyte nuclear architecture in a patient with LMNA gene mutation. J Neurol Sci 2008; 271:91-6.
25. Ozawa R, Hayashi YK, Ogawa M, Kurokawa R, Matsumoto H, Noguchi S, et al. Emerin-lacking mice show minimal motor and cardiac dysfunctions with nuclear associated vacuoles. Am J Pathol 2006; 168:907-[illegible]
26. Harding TM, Morano KA, Scott SV, Klionsky DJ. Isolation and characterization of yeast mutants in the cytoplasm to vacuole protein targeting pathway. J Cell Biol 1995; 131:591-602.
27. Klionsky DJ, Cregg JM, Dunn WA Jr, Emr SD, Sakai Y, Sandoval IV, et al. A unified nomenclature for yeast autophagy-related genes. Dev Cell 2003; 5:539-45.
28. Tanida I, Ueno T, Kominami E. LC3 conjugation system in mammalian autophagy. Int J Biochem Cell Biol 2004; 36:2503-18.
29. Dunn WA Jr, Cregg JM, Kiel JA, van der Klei IJ, Oku M, Sakai Y, et al. Pexophagy: the selective autophagy of peroxisomes. Autophagy 2005; 1:75-83.
30. Kim I, Rodriguez-Enriquez S, Lemasters JJ. Selective degradation of mitochondria by mitophagy. Arch Biochem Biophys 2007; 462:245-53.
31. Bernales S, Schuck S, Walter P. ER-phagy: selective autophagy of the endoplasmic reticulum. Autophagy 2007; [illegible]
32. Muchir A, [illegible] M, Mislow JM, McNally [illegible] Bonne G. Nuclear envelope alterations in fibroblasts from LGMD1B patients carrying nonsense [illegible] heterozygous or homozygous [illegible] in lamin A/C gene. Exp Cell Res 2003; 291:352-62.
33. Muchir A, Medioni J, Laluc M, Massart C, [illegible] van der Kooi AJ, et al. Nuclear envelope alterations in fibroblasts from patients with muscular dystrophy, cardiomyopathy and partial lipodystrophy carrying lamin A/C gene mutations. Muscle Nerve 2004; 30:444-50.
34. Kabeya Y, Mizushima N, Ueno T, Yamamoto A, Kirisako T, Noda T, et al. LC3, a mammalian homologue of yeast Apg8p, is localized in autophagosome membranes after processing. EMBO J 2000; 19:5720-8.
35. Mizushima N, Yamamoto A, Matsui M, Yoshimori T, Ohsumi Y. In vivo analysis of autophagy in response to nutrient starvation using transgenic mice expressing a fluorescent autophagosome marker. Mol Biol Cell 2004; 15:1101-11.
36. Xie Z, Klionsky DJ. Autophagosome formation: core machinery and adaptations. Nat Cell Biol 2007; 9:1102-9.
37. Young AR, Chan EY, Hu XW, Kochl R, Crawshaw SG, High S, et al. Starvation and ULK1-dependent cycling of mammalian Atg9 between the TGN and endosomes. J Cell Sci 2006; 119:3888-900.
38. Gutierrez MG, Munafo DB, Beron W, Colombo MI. Rab7 is required for the normal progression of the autophagic pathway in mammalian cells. J Cell Sci 2004; 117:2687-97.
39. Fillingham J, Keogh MC, Krogan NJ. GammaH2AX and its role in DNA double-strand break repair. Biochem Cell Biol 2006; 84:568-77.
40. Tanida I, Minematsu-Ikeguchi N, Ueno T, Kominami E. Lysosomal turnover, but not a cellular level, of endogenous LC3 is a marker for autophagy. Autophagy 2005; 1:84-91.
41. Nakagawa I, Amano A, Mizushima N, Yamamoto A, Yamaguchi H, Kamimoto T, et al. Autophagy defends cells against invading group A Streptococcus. Science 2004; 306:1037-40.
42. Kvam E, Goldfarb DS. Nucleus-vacuole junctions and piecemeal microautophagy of the nucleus in S. cerevisiae. Autophagy 2007; 3:85-92.
43. Kvam E, Goldfarb DS. Nucleus-vacuole junctions in yeast: anatomy of a membrane contact site. Biochem Soc Trans 2006; 34:340-2.
44. Krick R, Muehe Y, Prick T, Bremer S, Schlotterhose P, Eskelinen EL, et al. Piecemeal microautophagy of the nucleus requires the core macroautophagy genes. Mol Biol Cell 2008; 19:4492-505.
45. Marino G, Ugalde AP, Salvador-Montoliu N, Varela I, Quiros PM, Cadinanos J, et al. Premature aging in mice activates a systemic metabolic response involving autophagy induction. Hum Mol Genet 2008; 17:2196-211.
46. Pendas AM, Zhou Z, Cadinanos J, Freije JM, Wang J, Hultenby K, et al. Defective prelamin A processing and muscular and adipocyte alterations in Zmpste24 metalloproteinase-deficient mice. Nat Genet 2002; 31:94-9.
47. Arimura T, Helbling-Leclerc A, Massart C, Varnous S, Niel F, Lacene E, et al. Mouse model carrying H222P-Lmna mutation develops muscular dystrophy and dilated cardiomyopathy similar to human striated muscle laminopathies. Hum Mol Genet 2005; 14:155-69.
48. Sullivan T, Escalante-Alcalde D, Bhatt H, Anver M, Bhat N, Nagashima K, et al. Loss of A-type lamin expression compromises nuclear envelope integrity leading to muscular dystrophy. J Cell Biol 1999; 147:913-20.
49. Carra S, Seguin SJ, Lambert H, Landry J. HspB8 chaperone activity toward poly(Q)-containing proteins depends on its association with Bag3, a stimulator of macroautophagy. J Biol Chem 2008; 283:1437-44.

Human *PTRF* mutations cause secondary deficiency of caveolins resulting in muscular dystrophy with generalized lipodystrophy

Yukiko K. Hayashi,[1] Chie Matsuda,[2] Megumu Ogawa,[1] Kanako Goto,[1] Kayo Tominaga,[1] Satomi Mitsuhashi,[1] Young-Eun Park,[1] Ikuya Nonaka,[1] Naomi Hino-Fukuyo,[3] Kazuhiro Haginoya,[3,4] Hisashi Sugano,[5] and Ichizo Nishino[1]

[1]Department of Neuromuscular Research, National Institute of Neuroscience, National Center of Neurology and Psychiatry, Kodaira, Tokyo, Japan. [2]Neuroscience Research Institute, National Institute of Advanced Industrial Science and Technology, Tsukuba, Ibaraki, Japan. [3]Department of Pediatrics, Tohoku University School of Medicine, Sendai, Miyagi, Japan. [4]Department of Pediatric Neurology, Takuto Rehabilitation Center for Children, Sendai, Miyagi, Japan. [5]Department of Metabolic and Endocrine Medicine, Kochi Health Science Center, Kochi, Kochi, Japan.

Caveolae are invaginations of the plasma membrane involved in many cellular processes, including clathrin-independent endocytosis, cholesterol transport, and signal transduction. They are characterized by the presence of caveolin proteins. Mutations that cause deficiency in caveolin-3, which is expressed exclusively in skeletal and cardiac muscle, have been linked to muscular dystrophy. Polymerase I and transcript release factor (PTRF; also known as cavin) is a caveolar-associated protein suggested to play an essential role in the formation of caveolae and the stabilization of caveolins. Here, we identified *PTRF* mutations in 5 nonconsanguineous patients who presented with both generalized lipodystrophy and muscular dystrophy. Muscle hypertrophy, muscle mounding, mild metabolic complications, and elevated serum creatine kinase levels were observed in these patients. Skeletal muscle biopsies revealed chronic dystrophic changes, deficiency and mislocalization of all 3 caveolin family members, and reduction of caveolae structure. We generated expression constructs recapitulating the human mutations; upon overexpression in myoblasts, these mutations resulted in PTRF mislocalization and disrupted physical interaction with caveolins. Our data confirm that PTRF is essential for formation of caveolae and proper localization of caveolins in human cells and suggest that clinical features observed in the patients with *PTRF* mutations are associated with a secondary deficiency of caveolins.

Introduction

Caveolae are specific invaginations of the plasma membrane characterized by the presence of the protein caveolin. To date, 3 caveolin family members have been identified. Caveolin-1 and -2 are coexpressed in many cell types, such as endothelial cells, smooth muscle cells, fibroblasts, and adipocytes, and form a hetero-oligomeric complex (1). In contrast, caveolin-3 is expressed exclusively in skeletal and cardiac muscles (2). Caveolae are involved in several important cellular processes, including clathrin-independent endocytosis, regulation and transport of cellular cholesterol, and signal transduction (3, 4).

Polymerase I and transcript release factor (PTRF; also known as cavin) is a highly abundant caveolae component and is suggested to have an essential role in caveolar formation. In both mammalian cells and zebrafish, knockdown of PTRF leads to a reduction in caveolae density (5). Mice lacking PTRF do not have morphologically detectable caveolae, in addition to a markedly diminished protein expression of all 3 caveolin isoforms (6). Interestingly, PTRF-knockout mice mimic lipodystrophy in humans, demonstrating considerably reduced adipose tissue mass, high circulating triglyceride levels, glucose intolerance, and hyperinsulinemia (6).

Here we report that mutations in *PTRF* (GenBank accession no. 284119) caused a disorder presenting as generalized lipodystrophy and muscular dystrophy. We demonstrate that this condition was associated with deficiency and mislocalization of all 3 caveolin family members and reduction of caveolae structure.

Conflict of interest: The authors have declared that no conflict of interest exists.

Citation for this article: *J. Clin. Invest.* 119:2623–2633 (2009). doi:10.1172/JCI38660.

Results

Identification of PTRF mutations. Deficiency of caveolin-3 as a result of *CAV3* gene mutations is known to cause muscular dystrophy (7). We found 5 nonconsanguineous Japanese patients whose muscle showed caveolin-3 deficiency but without *CAV3* mutation among 2,745 muscular dystrophy specimens kept in the muscle repository of the National Center of Neurology and Psychiatry. Importantly, all 5 patients also had congenital generalized lipodystrophy (CGL; also known as Berardinelli-Seip syndrome). From the findings observed in lacking cells and animal models lacking PTRF (5, 6), we screened for *PTRF* mutations.

We identified 2 different frameshift mutations in all 5 patients examined: patients 1–4 (P1–P4) had the same homozygous c.696_697insC (p.K233fs) mutation in exon 2, and P5 harbored a compound heterozygous mutation of the same c.696_697insC and c.525delG (p.E176fs) in exon 2 (Figure 1A). The c.525delG mutation changes the last 275 amino acids to an unrelated 98-amino acid sequence, whereas c.696_697insC substitutes the last 158 amino acids with an unrelated 191-amino acid sequence (Figure 1B). Both mutations were not identified in the chromosomes of 200 Japanese control subjects.

In order to determine whether the common c.696_697insC mutation has the same haplotype, we examined 6 sets of single nucleotide polymorphisms (SNPs) within *PTRF*: rs2062213, rs8070945, rs963988, rs963987, rs963986, and rs9252. All 5 patients had the same haplotype for all 6 SNPs, which occurred homozygously (Table 1). During mutation screening, we found a novel 9-bp insertion polymorphism in the 3′ noncoding region

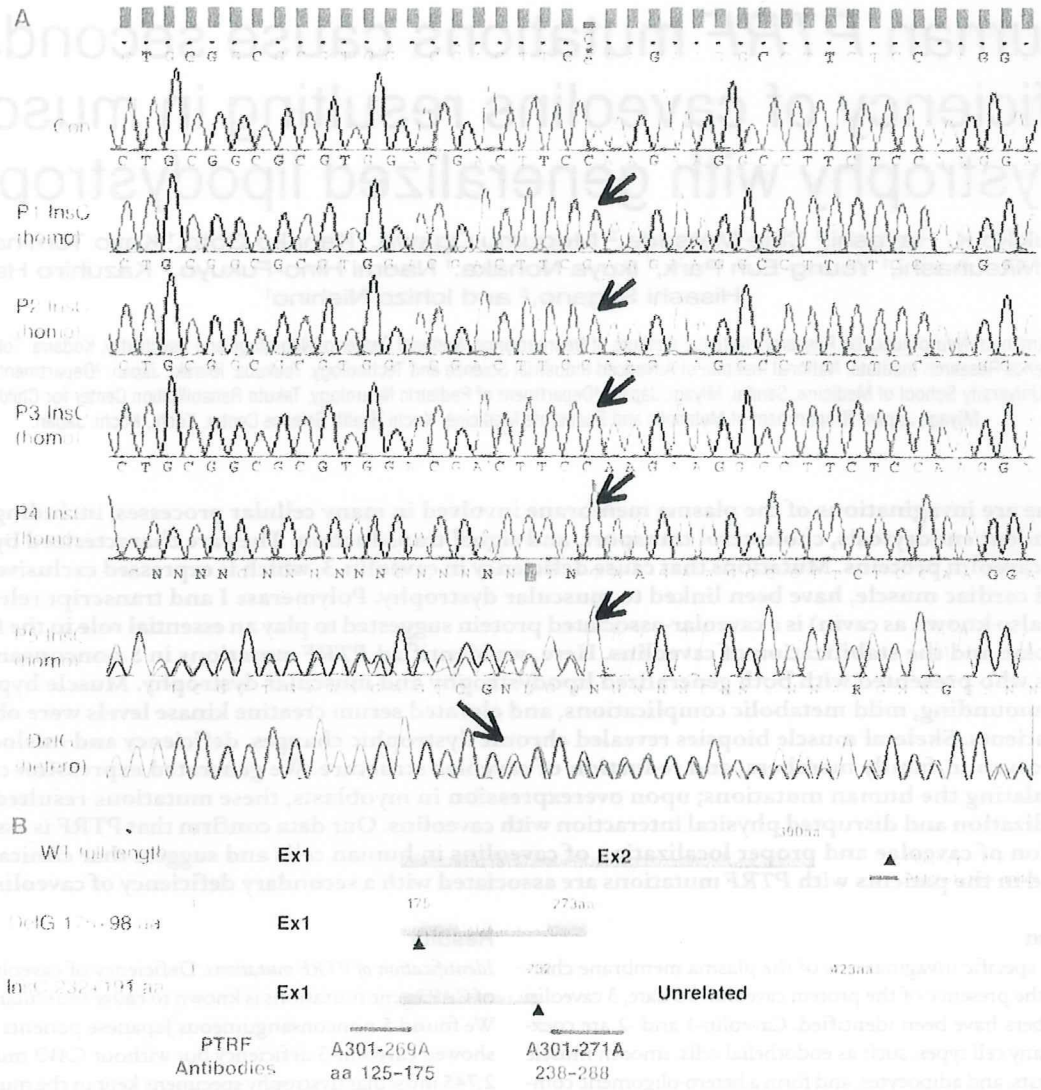

Figure 1

Mutations in *PTRF*. (**A**) All 5 patients had a homozygous or compound heterozygous mutation in *PTRF* (shown by arrows). P1–P4 had the same homozygous insertion mutation of c.696_697insC (InsC) in exon 2, whereas P5 had a compound heterozygous mutation of the same c.696_697insC insertion mutation and a deletion mutation of c.525delG (DelG) in exon 2. (**B**) Schema of the position of mutations in *PTRF*, putative proteins produced by mutations, and antibody recognition sites. The c.525delG mutant changes the last 275 amino acids to an unrelated 98–amino acid sequence, while the c.696_697insC mutant substitutes the last 158 amino acids with an unrelated 191–amino acid sequence.

of *PTRF* (c.1235_1236insTCTCGGCTC). This 9-bp insertion was found heterozygously in 26% and homozygously in 2% of Japanese control individuals. In P1–P5, none had this 9-bp insertion. We also examined 2 microsatellite markers (STS-W93348 and D17S1185) close to *PTRF* and found heterozygosity in the patients (Table 1). From these results, a founder effect may not be likely, although we could not completely rule out the possibility.

Mutation screening of the other genes associated with lipodystrophy and muscular dystrophy. From the clinical and pathological findings, we performed mutation screening for the genes associated with muscular dystrophy and lipodystrophy, including *CAV3*, *LMNA*, *AGPAT2*, *BSCL2*, *CAV1*, *PPARG*, *AKT2*, and *ZMPSTE24*. We found a heterozygous nucleotide change of c.1138G>A (p.D380N) in *BSCL2* in P1. This substitution was also identified heterozygously in 16% of Japanese control individuals, and we believe this to be a novel nonsynonymous SNP. For all the other genes examined, no other mutation was identified in P1–P5.

Clinical features of the patients with PTRF mutations. Clinical information for P1–P5 is summarized in Table 2. Common to all patients was the presence of muscular dystrophy and generalized lipodystrophy. However, despite having the same mutation, the patients' additional symptoms were variable. Generalized loss of subcutaneous adipose tissue in several areas, including the face, was noticed in infancy or early childhood. Hepatosplenomegaly, acromegaloid features, and umbilical prominence were often observed in the patients. No patient showed intellectual deficit or acanthosis nigricans. Patients presented with mild muscle weakness, but with hypertrophy of muscles (Figure 2A). Electrically silent percussion-induced

Table 1
Haplotype analysis

	P1	P2	P3	P4	P5	Control[A]
Intron 1, rs2062213	C/C	C/C	C/C	C/C	C/C	C/C (53%)
Intron 1, rs8070945	C/C	C/C	C/C	C/C	C/C	C/C (78%)
Intron 1, rs963988	G/G	G/G	G/G	G/G	G/G	G/G (33%)
Intron 1, rs963987	G/G	G/G	G/G	G/G	G/G	G/G (31%)
Intron 1, rs963986	G/G	G/G	G/G	G/G	G/G	G/G (34%)
Exon 2, 9-bp insertion[B]	no/no	no/no	no/no	no/no	no/no	no/no (72%)
Exon 2, rs9252[B]	C/C	C/C	C/C	C/C	C/C	C/C (78%)
STS-W93348 (bp)	251/253	251/253	251/253	251/253	251/253	251/253/264
D17S1185 (bp)	219/219	170/219	170/219	170/170	170/203	170/203/215/219/225/237

[A]Percentages denote the frequency of the haplotype in the HapMap JPT population. [B]Exon 2 is 3′ noncoding.

muscle mounding was characteristic. Cardiac arrhythmia, transient immunodeficiency, recurrent pneumonia, constipation, and chalasia were variably seen. Available laboratory data in the patients are summarized in Table 3. Metabolic complication was mild, and none of our patients showed marked elevation of fasting glucose levels. The result of oral glucose tolerance tests revealed moderate fasting hyperinsulinemia in P1 and P2 associated with glucose intolerance in P2, but normal levels in P4 (Table 4). High triglyceremia was seen in P4 and P5. Serum creatine kinase (CK) levels were moderately elevated in all patients. Abdominal CT images of P4 revealed marked loss of subcutaneous and intra-abdominal fat (Figure 2, B and C). In addition, his body fat ratio, as determined by whole body dual energy X-ray absorptiometry, was 7.1% (Supplemental Table 1; supplemental material available online with this article; doi:10.1172/JCI38660DS1), while head fat was relatively preserved.

Clinical features of the heterozygous parents. There was no family history of muscular dystrophy or lipodystrophy in P1–P5. Genetic analysis revealed a heterozygous c.696_698insC mutation in both parents of P4. Clinically, both father and mother had hypertension requiring medication, whereas P4 was normotensive. Mild lipid metabolism abnormality and borderline glucose intolerance was also seen (Supplemental Table 2). DNA samples from the other parents were not available.

Loss of PTRF with deficiency or mislocalization of caveolins in skeletal muscle. Biopsied skeletal muscles from P1–P5 showed consistent findings, with chronic dystrophic changes including marked variation in muscle fiber size, increased number of fibers containing internalized nuclei, a few necrotic and regenerating fibers, and increased interstitial fibrosis (Figure 2D and Supplemental Figure 1). Intramuscular lipid droplets, as visualized by oil red O staining, were not increased (Figure 2D).

Immunohistochemistry demonstrated that the PTRF antibodies A301-269A and A301-271A (which recognize the N- and C-terminal regions of the protein, respectively; Figure 1B) showed sarcolemmal membrane staining of muscle fibers, with stronger immunoreaction at intramuscular blood vessels in control muscles (Figure 3A). Caveolin-3 was clearly observed at sarcolemma, whereas caveolin-1 and -2 were present only in blood vessels. In contrast, muscles from P1–P5 showed barely detectable immunoreaction to both PTRF antibodies (Figure 3A). Caveolin-3 immunoreactivity was greatly reduced in the sarcolemma, but cytoplasmic staining was remarkably increased. This caveolin-3 staining pattern was similar to that seen in the patients with muscular dystrophy

Table 2
Clinical summary

	P1	P2	P3	P4	P5
Age/sex	8-yr-old female	14-yr-old female	10-yr-old male	27-yr-old male	24-yr-old male
Height, body weight	124 cm, 21.3 kg	149 cm, 40.5 kg	NA	164 cm, 49.0 kg	152 cm, 40 kg
Lipodystrophy	Generalized	Generalized	Generalized	Generalized	Generalized
Mental retardation	No	No	No	No	No
Acanthosis nigricans	No	No	No	No	No
Liver/spleen	Hepatosplenomegaly	Fatty liver	NA	Hepatosplenomegaly	No
Endocrine abnormalities	Reduced growth hormone secretion	NA	NA	Accelerated bone age, acromegaloid features, no androgynism	Acromegaloid features, no androgynism
Muscle weakness	Distal dominant	No	No	Generalized	Distal dominant
Muscle mounding	Positive	NA	NA	Positive	Positive
Other muscle symptoms	Muscle hypertrophy	Myalgia, muscle stiffness	NA	Muscle hypertrophy	Muscle hypertrophy
Cardiac symptoms	Arrhythmia	No	No	Atrial fibrillation	No
Skeletal abnormalities	Lordosis, Contractures (ankles, shoulders, fingers)	No	No	Scoliosis, contractures (ankles)	Scoliosis
Other symptoms	Constipation	Transient IgA deficiency, recurrent pneumonia	Nephrosis	Umbilical prominence, renal stones	Recurrent pneumonia, chalasia, constipation

NA, not available.

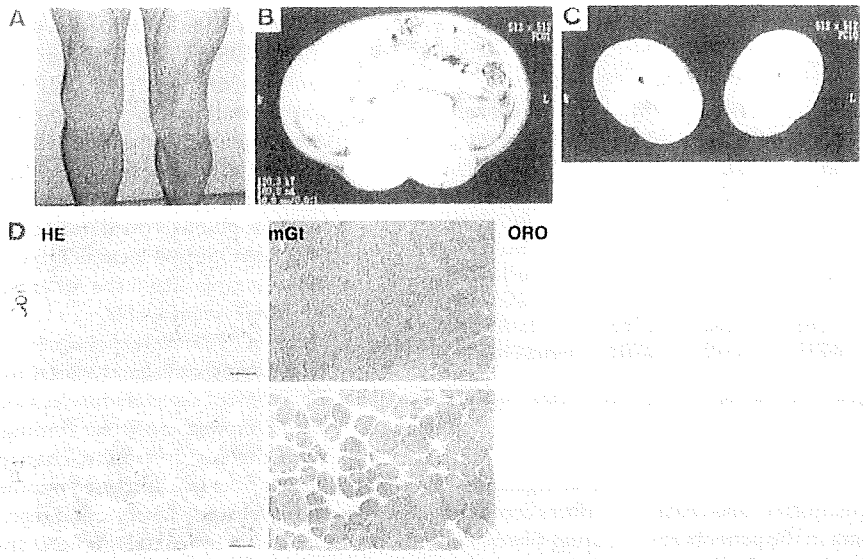

Figure 2
Muscle hypertrophy and dystrophic changes. (**A**) Prominent musculature feature of legs in P5. (**B** and **C**) CT images from P4 showed hypertrophy of paravertebral and thigh muscles with minimal subcutaneous and intra-abdominal fat tissue. (**D**) H&E stain of biopsied skeletal muscle from P4 showed dystrophic changes, including marked variation in fiber size, enlarged fibers with internalized nuclei, endomysial fibrosis, and few necrotic and regenerating fibers. Intramuscular lipid droplets were not increased compared with control. mGt, modified Gomori trichrome; ORO, oil red O. Scale bars: 50 μm.

caused by *CAV3* mutations (data not shown). Similarly, dysferlin was decreased in the sarcolemma and mislocalized into the cytoplasm (data not shown), and the same pattern is also seen in muscles of individuals with *CAV3* mutations (8). Immunoreactivity to caveolin-1 and caveolin-2 in blood vessels was barely detectable in P1–P5 (Figure 3A). Other antibodies related to muscular dystrophy, including dystrophin, sarcoglycans, dystroglycans, emerin, merosin, and collagen VI, showed normal immunostaining patterns (data not shown).

Immunoblotting showed detection of PTRF as an approximately 50-kDa band in control muscles and 3T3 cells, which were used as a positive control. No band was detected in the muscle of P1–P5 (Figure 3B). Caveolin-3 was detected in all samples examined, but relative protein amount, determined using densitometry and normalized by myosin heavy chain (MHC), decreased in P1–P5 compared with control subjects (Figure 3C). The band for caveolin-2 was observed in control muscles and 3T3 cells, but was barely detectable in the muscles of P1–P5 (Figure 3B).

In order to determine mRNA expression of PTRF, RT-PCR was performed using total RNA extracted from biopsied skeletal muscles. Using primers designed to amplify whole coding region of mRNA, PTRF was amplified as a single transcript in control muscles. In contrast, no PCR product was amplified in P1–P5 (Figure 4A). To compare mRNA levels for caveolins, we performed quantitative RT-PCR and normalized results to GAPDH expression. The mRNA amounts of all 3 caveolin families in the patients' muscles were variable, but not markedly decreased, compared with control muscles (Figure 4, B and C). Preserved mRNA levels, but decreased protein amounts of caveolins, suggested destabilization of caveolin proteins when PTRF is lacking, as previously reported (9).

Loss of PTRF causes reduced caveolae formation in human muscles. Greatly reduced caveolae formation was previously reported in PTRF knockdown mammalian cells, zebrafish, and knockout mice (5, 9). Decreased caveolae number was also reported in skeletal muscle from limb girdle muscular dystrophy type 1C (LGMD1C) patients with *CAV3* mutations (10). We therefore examined muscle caveolae in P2 and P3 using electron microscopy. Plasma membrane of muscle fibers from both patients was nearly flat, and caveolae density was notably reduced, compared with control muscle (Figure 5). Caveolae formation in the intramuscular vascular smooth muscle cells was also remarkably reduced (data not shown).

Altered localization of mutant PTRF and reduced interaction with caveolins in transfected cells. In order to determine the intracellular localization of mutant PTRF, FLAG-tagged WT or 2 mutants (c.525delG and c.696_697insC) and T7-tagged caveolin-3 or -1 were cotransfected in C2C12 myoblasts and COS-7 cells. In C2C12 cells, WT PTRF was detected at the cell membrane and colocalized with caveolin-3 (Figure 6A). Interestingly, c.525delG was detected as intranuclear aggregations and was not observed at the cell membrane (Figure 6, A and B). Caveolin-3 was present only in cytoplasm, and did not merge with PTRF (Figure 6A). The c.696_697insC mutant was observed as microtubular filament network in cytoplasm and colocalized with β-tubulin (Figure 6B). This finding is consistent with the localization of the truncated $PTRF_{1-322}$, as described previously (9). Similar mislocalization and/or aggregation of transfected mutant PTRF was observed in COS-7 cells (data not shown).

Table 3
Laboratory data

Measurement	Reference range	P1	P2	P3	P4	P5
CK (IU/l)	56–244	1,374	542–2,253	2,000	554–1,545	645–2,630
Fasting glucose (mg/dl)	70–109	75	99	NA	93–116	102
HbA1c (%)	4.3–5.8	NA	NA	NA	5.0–5.4	NA
Total cholesterol (mg/dl)	130–220	164	NA	NA	185–267	218
Triglyceride (mg/dl)	50–150	93	NA	NA	143–450	359
LDL-C (mg/dl)	70–139	NA	NA	NA	188	NA
Leptin (ng/ml)	0.9–13.0	NA	NA	NA	0.6	NA
Adiponectin (μg/ml)	None	NA	NA	NA	1.05	NA

NA, not available.

Table 4
Oral glucose tolerance test of P1, P2, and P4

	Pre	30 min	60 min	120 min
P1				
Glucose (mg/dl)	75	98	69	62
IRI (μU/ml)	22.8	141.6	64.7	23.8
P2				
Glucose (mg/dl)	99	127	160	172
IRI (μU/ml)	20	53	65	80
P4				
Glucose (mg/dl)	93	124	140	70
CPR (ng/ml)[A]	2.8	5.9	8.3	5.5
IRI (μU/ml)	1.0	22.3	32.9	6.2

IRI, immunoreactive insulin; CPR, C-peptide immunoreactivity. [A]Reference range, 0.7–2.2 ng/ml.

We performed immunoprecipitation assay in order to examine the binding ability of PTRF and caveolins. WT PTRF was coimmunoprecipitated by anti-T7 antibody, and vice versa (Figure 6, C and D). The c.525delG mutant showed smaller molecular weight (estimated 30 kDa; Figure 1B), and no immunoprecipitated protein was detected by FLAG and T7 antibodies. The c.696_697insC mutant showed slightly larger molecular weight, and coimmunoprecipitated proteins were greatly reduced (Figure 6, C and D). These results suggest that mutant PTRFs cannot localize properly and lose their binding ability to caveolins even if they are produced.

Activation of myostatin and Akt signaling pathways in PTRF-deficient skeletal muscles. Caveolin-3 is suggested to have an important role for suppression of myostatin-mediated signaling in skeletal muscle (11). In order to determine the functions of mislocalized caveolin-3 in *PTRF* mutated cells, we performed quantitative RT-PCR for myostatin and immunoblotting analysis to examine phosphorylation status of Mad homolog 2/3 (p-Smad2/3), an intracellular effector of myostatin in skeletal muscles. In P1–P5, increased amounts of p-Smad2/3$^{S423/425}$ were observed in skeletal muscles, while myostatin mRNA levels were variable (Figure 7, A–C). Positive immunoreaction to p-Smad2/3 was detected in few myonuclei from muscle of patients with *PTRF* or *CAV3* mutations, but not in those from muscle of control subjects (data not shown). These results suggest that myostatin signaling is also activated in P1–P5.

Despite the activation of myostatin, a negative regulator of muscle growth, the patients showed hypertrophy of muscles. Since Akt (also known as protein kinase B) is known as the key molecule to regulate muscle mass (12), we examined p-Akt^{T308} and p-Akt^{S473} by immunoblotting analysis. p-Akt was elevated in the muscle of P1–P5 compared with controls, except for p-Akt^{S473} in P2 (Figure 7, D–F). This result suggests that Akt pathway is activated, probably through an as-yet-unidentified mechanism, and could contribute to the muscle hypertrophy observed in P1–P5.

Neuronal NOS activity is variable and mildly increased in PTRF-deficient skeletal muscles. Caveolin-3 is known to interact with and negatively regulate the catalytic activity of neuronal NOS (nNOS) in skeletal muscle (13); this notion is supported by the finding of increased nNOS activity in muscle of transgenic mice expressing mutant caveolin-3 (14). We thus examined nNOS expression and its activity in muscles from patients with mutations in *PTRF* or *CAV3* compared with those from age-matched controls. The immunoreactivity of nNOS was seen in sarcolemma and cytoplasm of each muscle fiber with variable intensity, but no obvious difference was seen between patients and controls (Figure 3A). Immunoblotting analysis also revealed comparable amounts of nNOS (Figure 3, B and D). In order to examine nNOS activity of each muscle fiber, we performed NADPH diaphorase (NDP) activity assay. The intensity of NDP staining appeared variable among muscle fibers and was slightly increased in patients with mutations in *PTRF* or *CAV3* compared with age-matched controls (Figure 8).

Discussion

Lipodystrophy is a heterogeneous group of disorders characterized by loss of adipose tissue from the body. The degree of fat loss varies from small areas to near-complete absence of adipose tissue. The extent of fat loss usually determines clinical severity and metabolic complications, such as insulin resistance and high levels of serum triglycerides.

Several genes responsible for inherited lipodystrophy have been identified. CGL is an autosomal-recessive disorder, with most patients presenting soon after birth with severe insulin resistance and elevated serum triglycerides. CGL1 is caused by mutations in *AGPAT2* on chromosome 9q34, which encodes 1-acylglycerol-3-phospate-O-acyltransferase 2, an enzyme involved in the biosynthesis of triacylglycerol and glycerophospholipids (15). CGL2 is caused by mutations in *BSCL2* on chromosome 11q13, which encodes a functionally unknown protein named seipin (16). Recently, mutations in *CAV1* on chromosome 7q31 have been reported to cause generalized (i.e., CGL3) and partial lipodystrophy (17, 18).

Several causative genes for autosomal-dominant familial partial lipodystrophy are known: *LMNA* on chromosome 1q21 (19), *ZMPSTE24* on chromosome 1p34 (20), *AKT2* on chromosome 19q13 (21), *PPARG* on chromosome 3p25 (22), and *LMNB2* on chromosome 19q1 (23). Nevertheless, many patients clinically diagnosed with lipodystrophy carry no mutation in the known genes, suggesting the presence of other causative genes.

Here we conclude that *PTRF* mutations can cause CGL. In our series, patients showed generalized loss of adipose tissue from infancy or early childhood. Because PTRF is reported to colocalize with hormone-sensitive lipase and translocate to the nucleus in the presence of insulin in adipocytes (24), it could be surmised that PTRF plays an important role in lipid metabolism and insulin-regulated gene expression. Interestingly, metabolic complications were milder in patients with *PTRF* mutations than in patients with CGL1 and CGL2, and these were observed only in the elder patients. Although we could not examine the status of caveolae and caveolins in adipose tissues, the secondary deficiency of caveolins might have an important role in the process of lipodystrophy, since *CAV1* mutation can cause lipodystrophy in both humans and mice (17, 18, 25). Notably, the heterozygous parents had mild metabolic disorders, but a robust conclusion could not be reached, as a limited number of the heterozygous carriers of the *PTRF* mutation were available to us. Further investigation is needed to determine the effect of haploinsufficiency of PTRF.

Skeletal muscle symptoms with serum CK elevation represent another common symptom in patients with *PTRF* mutations. The clinical and pathological findings are very similar to those observed in patients with *CAV3* mutation (7, 26–28), although P1–P5 had no *CAV3* mutations. The secondary loss of caveolin-3 in the sarcolemma may contribute to the muscle phenotype. Moreover, serum CK elevation may be a good laboratory marker for diagnosis of lipodystrophy patients with *PTRF* mutations.

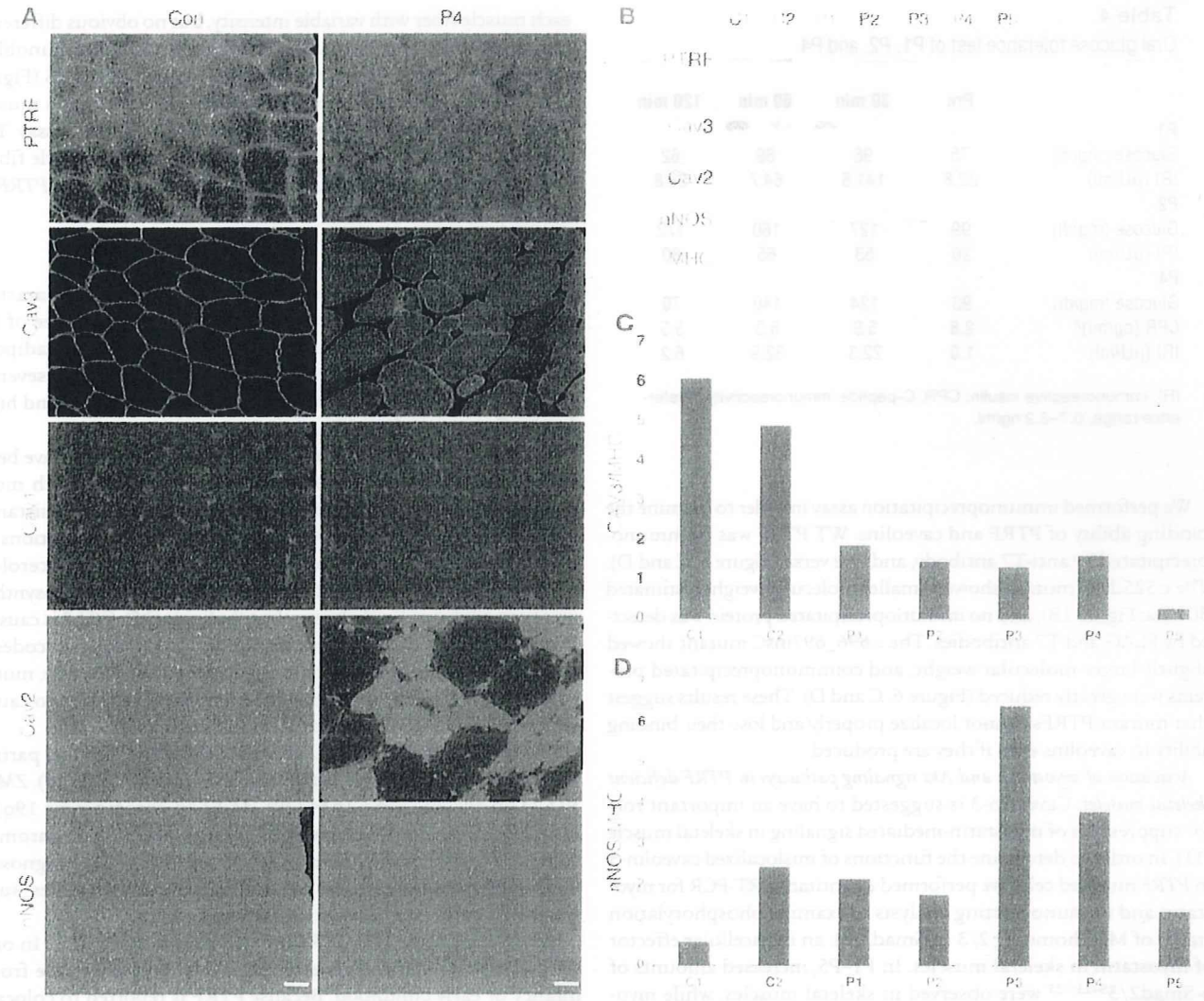

Figure 3

Loss of PTRF is associated with deficiency and mislocalization of caveolins in muscle. (**A**) In control muscle, PTRF was clearly seen in sarcolemma as strongly staining blood vessels. Caveolin-3 (Cav3) was clearly visible at sarcolemma, and caveion-1 and -2 stained intramuscular blood vessels. The muscle of P4 was negative for PTRF. Membrane staining of caveolin-3 was reduced with increased cytoplasmic staining, and caveolin-1 and -2 were barely detectable. Immunoreactivity of nNOS varied between muscle fibers, but was not markedly different between control and patient muscle. Scale bar: 50 μm. (**B**) Immunoblotting analysis of skeletal muscles. 3T3 cells were used as a positive control. PTRF and caveolin-2 were seen only in the muscles of 2 control subjects and in 3T3 cells, and were barely detectable in the muscles of P1–P5. The bands for caveolin-3 and nNOS were variably seen. (**C** and **D**) Quantification of immunoreactive bands was performed by densitometric analysis and normalized with MHC. In P1–P5, relative amounts of caveolin-3 decreased compared with control subjects (**C**), whereas nNOS amounts varied (**D**).

Caveolin-3 was previously reported to have an important role in inhibition of myostatin signaling by suppressing activation of its type I receptor. In mutant *Cav3* transgenic mice, loss of caveolin-3 causes muscular atrophy with increased p-Smad2, and this muscle atrophy can be rescued by myostatin inhibition (11). Consistent with the secondary reduction of caveolin-3, skeletal muscles from P1–P5 showed increased amounts of p-Smad2/3. Unexpectedly, however, muscle hypertrophy was seen in these patients.

The Akt pathway, when activated, is known to promote protein synthesis, stimulate muscle hypertrophy, and inhibit atrophy-related gene expression by phosphorylating FoxO transcription factors (12). This pathway is also known to play a pivotal role in the regulation of glucose transport and glycogen synthesis in skeletal muscle cells. Akt is activated by insulin, various growth factors, nutrients, and exercise, whereas it is negatively regulated by myostatin and cytokines. Akt is phosphorylated at T308 by phosphoinositide-dependent kinase and at S473 by mammalian target of rapamycin in association with rictor. The increase in phosphorylated Akt in the muscle of P1–P5 may explain, at least in part, the muscle hypertrophy observed. Akt pathway activation might be associated with the metabolic complications observed in P1–P5. However, the upregulation of myostatin observed is contradictory to the established knowledge on muscle hypertrophy. This would be worthwhile to investigate in future studies, in order to

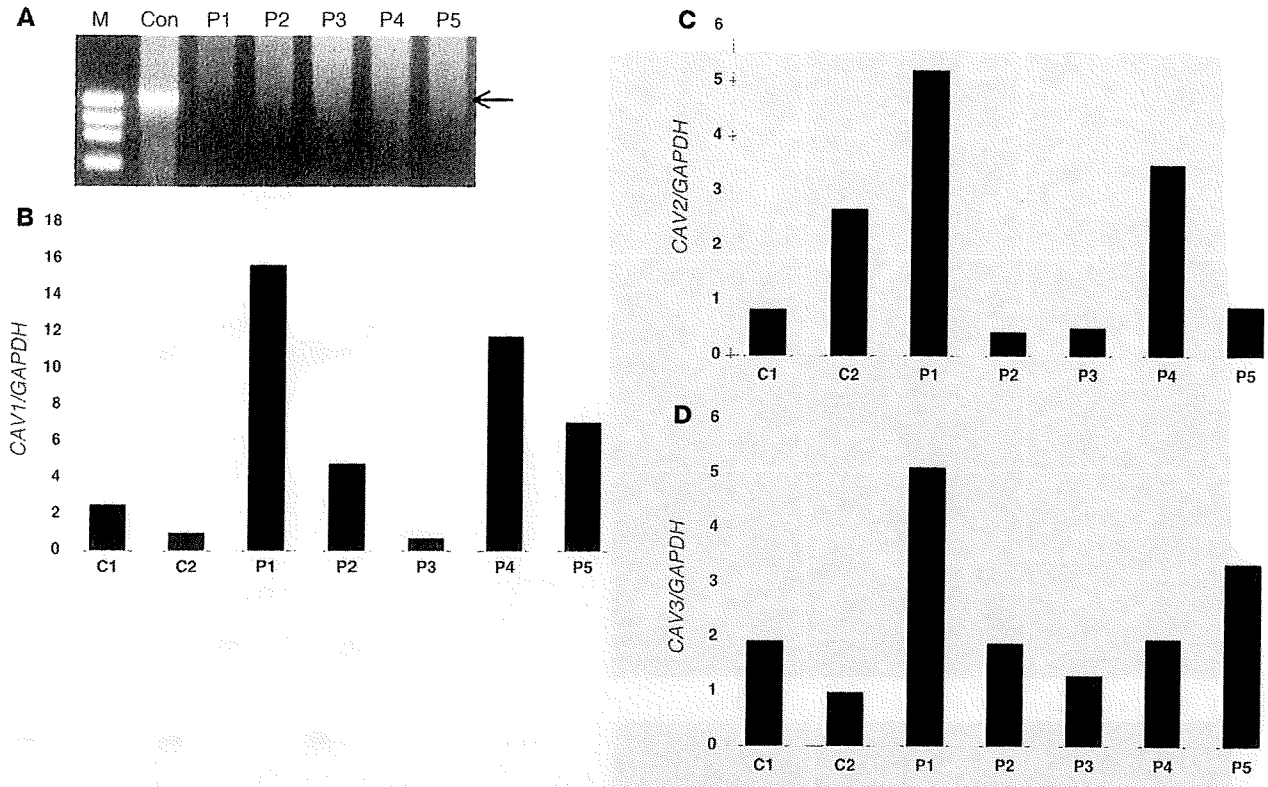

Figure 4
mRNA expression of PTRF in skeletal muscle, and quantitative RT-PCR of mRNAs for caveolins. (**A**) RT-PCR analysis revealed a single band for *PTRF* mRNA (arrow) in a control subject, but no detectable product was seen in P1–P5. M, marker. (**B–D**) By quantitative RT-PCR, mRNA for *CAV1*, *CAV2*, and *CAV3* normalized with *GAPDH* expression was not decreased in P1–P5.

elucidate the role of PTRF deficiency in muscle hypertrophy and related signaling pathway.

In addition to lipodystrophy and muscular dystrophy, P1–P5 had various other symptoms, whose association to *PTRF* mutation might be difficult to ascertain at this time. For example, 2 of 5 patients had arrhythmia. Although we could not examine the expression of caveolins in cardiac muscle, this cardiac abnormality may be caused by secondary deficiency of caveolins in heart, as cardiac involvement was previously reported in patients with *CAV3* mutations and in mutant mice with double knockout of *Cav1* and *Cav3* (29–33).

Remarkable reduction in expression of caveolin-1 and -2 with decreased caveolae density was observed in vascular endothelial cells in P1–P5. There was no obvious symptom related to vascular endothelial blood vessels in the patients; however, further careful investigation is necessary in order to determine the involvement of endothelial cells, which was observed in *Cav1* knockout mice (34). The severe constipation and esophageal dilatation observed in the patients might be associated with dysfunction of caveolin-1 in smooth muscle cells, as *Cav1* knockout mice had alteration of smooth muscles and interstitial cells of Cajal, the pacemaker cells of the muscle layers of the gastrointestinal tract (35).

Caveolae was previously suggested to have a role in the internalization of growth hormone in vitro (36). The acromegaloid features, accelerated bone age, or abnormal growth hormone activity observed in 3 patients in the present study might be associated with reduced caveolae formation. Recurrent pneumonia and transient immunodeficiency observed in 2 patients were also noted, although the pathomechanisms are still unknown. Further detailed studies are needed to elucidate the roles of PTRF; however,

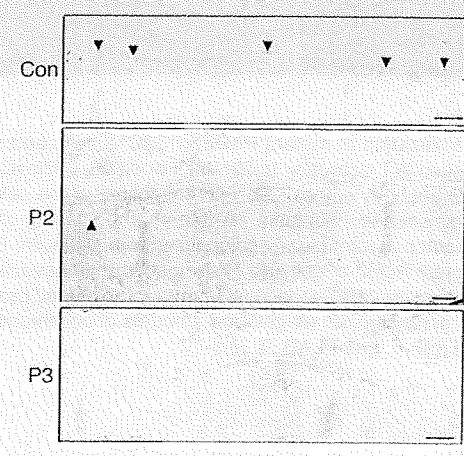

Figure 5
Reduced caveolae formation in skeletal muscle, as assessed by electron microscopy. In control muscle, an abundance of caveolae (arrowheads) was observed close to the plasma membrane. Plasma membrane of muscle fibers from P2 and P3 was nearly flat, and caveolae density was greatly reduced compared with that of control muscle. Only a few caveolae were seen in P2. Scale bars: 200 nm.